Integrating Prior Knowledge in Contrastive Learning with Kernel

Benoit Dufumier [1 2]   Carlo Alberto Barbano [2 3]   Robin Louiset [1 2]   Edouard Duchesnay [1]   Pietro Gori [2]

Abstract

Data augmentation is a crucial component in unsupervised contrastive learning (CL). It determines how positive samples are defined and, ultimately, the quality of the learnt representation. In this work, we open the door to new perspectives for CL by integrating prior knowledge, given either by generative models–viewed as prior representations– or weak attributes in the positive and negative sampling. To this end, we use kernel theory to propose a novel loss, called *decoupled uniformity*, that i) allows the integration of prior knowledge and ii) removes the negative-positive coupling in the original InfoNCE loss. We draw a connection between contrastive learning and conditional mean embedding theory to derive tight bounds on the downstream classification loss. In an unsupervised setting, we empirically demonstrate that CL benefits from generative models to improve its representation both on natural and medical images. In a weakly supervised scenario, our framework outperforms other unconditional and conditional CL approaches. Source code is available at this https URL.

1. Introduction

Contrastive Learning (CL) (Becker & Hinton, 1992; Bromley et al., 1993; Oord et al., 2019; Bachman et al., 2019; Chen et al., 2020a) is a paradigm designed for self-supervised representation learning which has been applied to unsupervised (Chen et al., 2020a;c), weakly supervised (Tsai et al., 2022; Dufumier et al., 2021) and supervised problems (Khosla et al., 2020). It gained popularity during the last years by achieving impressive results in the unsupervised setting on standard vision datasets (*e.g.* ImageNet) where it almost matched the performance of its supervised counterpart (Chen et al., 2020a; He et al., 2020).

The objective in CL is to increase the similarity in the representation space between *positive* samples (semantically close), while decreasing the similarity between *negative* samples (semantically distinct). Despite its simple formulation, it requires the definition of a similarity function (that can be seen as an energy term (LeCun & Huang, 2005)),and of a rule to decide whether a sample should be considered positive or negative. Similarity functions, such as the Euclidean scalar product (*e.g.* InfoNCE (Oord et al., 2019)), take as input the latent representations of an encoder $f \in \mathcal{F}$, such as a CNN (Chen et al., 2020b) or a Transformer (Caron et al., 2021) for vision datasets.

In supervised settings (Khosla et al., 2020), positives are simply images belonging to the same class while negatives are images belonging to different classes. In unsupervised problems (Chen et al., 2020a), since labels are unknown, positives are usually defined as transformed versions (*views*) of the same original image (a.k.a. the anchor) and negatives are the transformed versions of all other images. As a result, the augmentation distribution $\mathcal{A}$ used to sample both positives and negatives is crucial (Chen et al., 2020a) and it conditions the quality of the learnt representation. The most-used augmentations for visual representations involve aggressive crop and color distortion. Cropping induces representations with high occlusion invariance (Purushwalkam & Gupta, 2020) whereas color distortion may avoid the encoder f to take a shortcut (Chen et al., 2020a) while aligning positive samples and therefore to fall into the simplicity bias (Shah et al., 2020).

Nevertheless, learning a representation that mainly relies on augmentations comes at a cost: both crop and color distortion induce strong biases in the final representation (Purushwalkam & Gupta, 2020). Specifically, dominant objects inside images can prevent the model from learning features of smaller objects (Chen et al., 2021) (which is not apparent in object-centric datasets such as ImageNet) and few, irrelevant and easy-to-learn features, that are shared among views, are sufficient to collapse the representation (Chen et al., 2021) (a.k.a feature suppression). Finding the right augmentations in other visual domains, such as medical imaging, remains an open challenge (Dufumier et al., 2021) since we need to find transformations that preserve semantic anatomical structures (e.g. discriminative between pathological and healthy) while removing unwanted noise. If
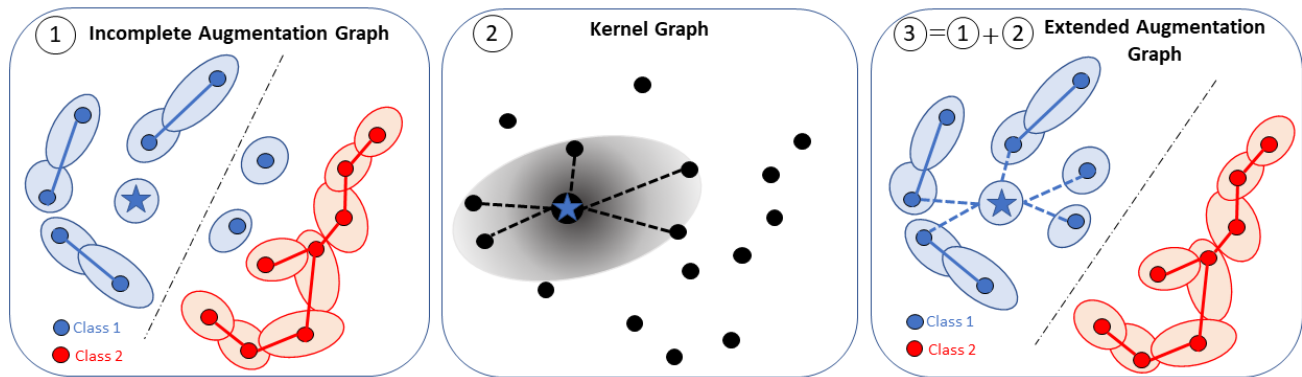
---

[1]NeuroSpin, CEA, Université Paris-Saclay [2]LTCI, Télécom Paris, IPParis [3]University of Turin. Correspondence to: Benoit Dufumier <benoit.dufumier@cea.fr>.

Figure 1: Illustration of the proposed method. Each point is an original image $\bar{x}$. Two points are connected if they can be transformed into the same augmented image using a distribution of augmentations $\mathcal{A}$. Colors represent semantic (unknown) classes and light disks represent the support of augmentations, $\mathcal{A}(\cdot|\bar{x})$, for each sample $\bar{x}$. From an incomplete augmentation graph (1) where intra-class samples are not connected (e.g. $\mathcal{A}$ is insufficient or not adapted), we reconnect them using a kernel defined on prior information (either learnt with generative model, viewed as feature extractor, or given as auxiliary attributes). The extended augmentation graph (3) is the union between the (incomplete) augmentation graph (1) and the kernel graph (2). In (2), the gray disks indicate the set of points $\bar{x}'$ that are close to the anchor (blue star) in the kernel space.

the augmentations are too weak or inadequate to remove irrelevant signal w.r.t. a discrimination task, then how can we define positive and negative samples?

In our work, we propose to integrate *prior information*, learnt from generative models (viewed as features extractor or prior representation) or given as auxiliary weak attributes (*e.g.,* phenotypes of participants for medical images), into contrastive learning, to make it less dependent on data augmentation. Using the theoretical understanding of CL through the augmentation graph, we make the connection with kernel theory and introduce a novel loss with theoretical guarantees on downstream performance. This loss additionally benefits from the decoupling effect between positive and negative samples that affects InfoNCE-based frameworks (Yeh et al., 2022). Prior information is integrated into the proposed decoupled contrastive loss using a kernel. In the unsupervised setting, we leverage pre-trained generative models, such as GAN (Goodfellow et al., 2014) and VAE (Kingma & Welling, 2013), to learn *a prior representation* of the data. We provide a solution to the feature suppression issue in CL (Chen et al., 2021) and also demonstrate SOTA results with weaker augmentations on visual benchmarks (both on natural and medical images). In the weakly supervised setting, we use instead auxiliary image attributes as prior knowledge (e.g. birds color or size) and we show better performance than previous conditional formulations based on these attributes (Tsai et al., 2022). In summary, we make the following contributions:

1. We propose a new decoupled contrastive loss which allows the integration of prior information, given as auxiliary attributes or learnt from generative models, into the positive and negative sampling.

2. We derive general guarantees, relying on weaker assumptions than existing theories, on the downstream classification task especially in the finite-samples case.

3. We empirically show that our framework performs competitively with small batch size and benefits from the latest advances of generative models to learn a better representation than existing CL methods.

4. We show that we achieve SOTA results in the unsupervised and weakly supervised setting.

2. Related Works

In a weakly supervised setting, recent studies (Dufumier et al., 2021; Tsai et al., 2022) about CL have shown that positive samples can be defined conditionally to an auxiliary attribute in order to improve the final representation, in particular for medical imaging (Dufumier et al., 2021). From an information bottleneck perspective, these approaches essentially compress the representation to be predictive of the auxiliary attributes. This might harm the performance of the model when the attributes are too noisy to accurately approximate the true labels of a given downstream task.

In an unsupervised setting, recent approaches (Dwibedi et al., 2021; Zheng et al., 2021a;b; Li et al., 2021) used the encoder f, learnt during optimization, to extend the positive sampling procedure to other views of different instances (*i.e.* distinct from the anchor) that are close to the anchor in the latent space. In order to avoid representation collapse, multiple instances of the same sample (Azizi et al., 2021), a support set (Dwibedi et al., 2021), a momentum encoder (Li et al., 2021) or another small network (Zheng et al., 2021a) can be used to select the positive samples. In clustering

approaches (Li et al., 2021; Caron et al., 2020), distinct instances with close semantics are attracted in the latent space using prototypes. These prototypes can be estimated through K-means (Li et al., 2021) or Sinkhorn-Knopp algorithm (Caron et al., 2020). All these methods rely on the past representation of a network to improve the current one. They require strong augmentations and they essentially assume that the closest points in the representation space belong to the same latent class in order to better select the positives. This inductive bias is still poorly understood from a theoretical point of view (Saunshi et al., 2022) and may depend on the visual domain.

Our work also relates to generative models for learning representations. VAEs (Kingma & Welling, 2013) learn the data distribution by mapping each input to a Gaussian distribution that we can easily sample from to reconstruct the original image. GANs (Goodfellow et al., 2014), instead, sample directly from a Gaussian distribution to generate images that are classified by a discriminator in a min-max game. The discriminator representation can then be used (Radford et al., 2016) as feature extractor. Other models (ALI (Dumoulin et al., 2017), BiGAN (Donahue et al., 2017) and BigBiGAN (Donahue & Simonyan, 2019)) learn simultaneously a generator and an encoder that can be used directly for representation learning. All these models do not require particular augmentations to model the data distribution but they perform generally poorer than recent discriminative approaches (Zhai et al., 2019; Chen et al., 2020b) for representation learning. A first connection between generative models and contrastive learning has emerged very recently (Jahanian et al., 2022). In (Jahanian et al., 2022), authors study the feasibility of learning effective visual representations using only generated samples, and not real ones, with a contrastive loss. Their empirical analysis is complementary to our work. Here, we leverage the representation capacity of the generative models, rather than their generative power, to learn prior representation of the data.

3. CL with Decoupled Uniformity

Problem setup. The general problem in contrastive learning is to learn a data representation using an encoder $f \in \mathcal{F} : \mathcal{X} \to \mathbb{S}^{d-1}$ that is pre-trained with a set of n original samples $(\bar{x}_i)_{i \in [1..n]} \in \bar{\mathcal{X}}$, sampled from the data distribution $p(\bar{x})$[1] These samples are transformed to generate *positive samples* (*i.e.*, semantically similar to $\bar{x}$) in $\mathcal{X}$, space of augmented images, using a distribution of augmentations $\mathcal{A}(\cdot|\bar{x})$. Concretely, for each $\bar{x}_i$, we can sample views of $\bar{x}_i$ using $x \sim \mathcal{A}(\cdot|\bar{x}_i)$ (*e.g.*, by applying color jittering, flip or crop with a given probability). For consistency, we assume $\mathcal{A}(\bar{x}) = p(\bar{x})$ so that the distributions $\mathcal{A}(\cdot|\bar{x})$

and $p(\bar{x})$ induce a marginal distribution $p(x)$ over $\mathcal{X}$. Given an anchor $\bar{x}_i$, all views $x \sim \mathcal{A}(\cdot|\bar{x}_j)$ from different samples $\bar{x}_{j \neq i}$ are considered as *negatives*. Once pre-trained, the encoder f is fixed and its representation $f(\bar{\mathcal{X}})$ is evaluated through linear evaluation on a classification task using a labeled dataset $\mathcal{D} = \{(\bar{x}_i, y_i)\} \in \bar{\mathcal{X}} \times \mathcal{Y}$ where $\mathcal{Y} = [1..K]$, with K the number of classes.

Linear evaluation. To evaluate the representation of f on a classification task, we train a linear classifier $g(\bar{x}) = W f(\bar{x})$ (f fixed) that minimizes the multi-class classification loss.

Negative-positive coupling (NPC) in CL. The popular InfoNCE loss (Poole et al., 2019; Oord et al., 2019), often used in CL, (asymptotically) imposes 1) alignment between positives and 2) uniformity between the views ($x \overset{\text{i.i.d.}}{\sim} \mathcal{A}(\cdot|\bar{x})$) of all instances $\bar{x}$ (Wang & Isola, 2020)– two properties that correlate well with downstream performance. However, by imposing uniformity between *all* views, we essentially try to both attract (alignment) and repel (uniformity) positive samples and therefore we cannot achieve a perfect alignment *and* uniformity, as noted in (Wang & Isola, 2020). One solution is to remove the positive pairs in the denominator of InfoNCE, as proposed by (Yeh et al., 2022) with DC, which notably allows to drastically reduce the batch size in InfoNCE-based frameworks. Here, we propose another (unexplored) solution by imposing uniformity only between centroids, defined as the average between several views of the same image $\bar{x}_i$, *i.e.*, $\mu_{\bar{x}_i} = \mathbb{E}_{x \sim \mathcal{A}(\cdot|\bar{x}_i)} f(x)$.

Integration of prior. Unsupervised CL only relies on data augmentation to learn representations, even if we may have access to prior knowledge $z(\bar{x}_i)$ about the original image $\bar{x}_i$ that can improve the final representation. Here, $z(\bar{x}_i)$ designates either a weak attribute or a prior representation given by a generative model. To this end, we propose to use a kernel $\bar{K}(z(\bar{x}_i), z(\bar{x}_j))$ between these priors in order to better estimate the centroids $(\mu_{\bar{x}_i})_{i \in [1..n]}$ of the original samples $(\bar{x}_i)_{i \in [1..n]}$. Intuitively, we want embeddings $(f(\bar{x}_i), f(\bar{x}_j))$ to be close if the priors $(z(\bar{x}_i), z(\bar{x}_j))$ are close in the kernel space. We rely on conditional mean embedding theory to use a new kernel-based estimator of these centroids (see Section 3.3.2).

Our solution. We propose to solve both NPC issue in InfoNCE loss and the integration of prior in CL by optimizing a loss relying only on centroids $(\mu_{\bar{x}_i})_{i \in [1..n]}$, that we called Decoupled Uniformity:

$$\mathcal{L}_{unif}^{de}(f) = \log \mathbb{E}_{p(\bar{x})p(\bar{x}')} e^{-||\mu_{\bar{x}} - \mu_{\bar{x}'}||^2} \qquad (1)$$

Here, we do not repel views from the same image anymore (solving negative-positive coupling issue) and we can integrate prior knowledge with kernel-based estimator of the centroids (solving prior integration). This loss essentially repels distinct centroids $\mu_{\bar{x}}$ through an average pairwise Gaussian potential. It implicitly optimizes alignment be-

---

[1] With an abuse of notation, we define it as $p(\bar{x})$ instead than $p_{\bar{X}}$ to simplify the presentation, as it is common in the literature

tween positives through the maximization[2] of $||\mu_{\bar{x}}||$, so **we do not need to explicitly add an alignment term**.

We first derive theoretical guarantees in the finite-samples case for this loss before introducing our main theorems.

Supervised risk. While previous analysis (Wang et al., 2022; Saunshi et al., 2019) generally used the mean cross-entropy loss (as it has closer analytic form with InfoNCE), we use a supervised loss closer to decoupled uniformity with the same guarantees as the mean cross-entropy loss (see Appendix C.1). Notably, the geometry of the representation space at optimum is the same as cross-entropy and Sup-Con (Khosla et al., 2020) and we can theoretically achieve perfect linear classification.

Definition 3.1. (Downstream supervised loss) For a given downstream task $\mathcal{D} = \bar{\mathcal{X}} \times \mathcal{Y}$, we define the classification loss as: $\mathcal{L}_{sup}(f) = \log \mathbb{E}_{y,y' \sim p(y)p(y')} e^{-||\mu_y - \mu_{y'}||^2}$, where $\mu_y = \mathbb{E}_{p(\bar{x}|y)} \mu_{\bar{x}}$ are averaged representation of samples belonging to the same class y.

This loss depends on centroids $\mu_{\bar{x}}$ rather than $f(\bar{x})$. Empirically, it has been shown (Foster et al., 2021) that performing features averaging gives better performance on the downstream task.

3.1. $\mathcal{L}_{unif}^{de}(f)$ solves the NPC problem

Definition 3.2. (Finite-samples estimator) For n samples $(\bar{x}_i)_{i \in [1..n]} \overset{i.i.d.}{\sim} p(\bar{x})$, the (biased) empirical estimator of $\mathcal{L}_{unif}^{de}(f)$ is: $\hat{\mathcal{L}}_{unif}^{de}(f) = \log \frac{1}{n(n-1)} \sum_{i \neq j} e^{-||\mu_{\bar{x}_i} - \mu_{\bar{x}_j}||^2}$. It converges in law to $\mathcal{L}_{unif}^{de}(f)$ with rate $O\left(n^{-1/2}\right)$. Proof in Appendix E.1

To show that $\hat{\mathcal{L}}_{unif}^{de}$ imposes alignment between positives and it solves the NPC problem in InfoNCE, we perform a gradient analysis, following (Yeh et al., 2022). We compute the gradients w.r.t. the view $z_k^{(v)} = f(x_k^{(v)})$ ($k \in [1..n]$ and $v \in \{1, 2\}$ for 2 views, proof in Appendix E.2):

$$\nabla_{z_k^{(v)}} \hat{\mathcal{L}}_{unif}^{de} = \underbrace{-2w_k \mu_{\bar{x}_k}}_{\text{align hard positives}} + \underbrace{2 \sum_{j \neq k} w_{k,j} \mu_{\bar{x}_j}}_{\text{repel hard negatives}} \quad (2)$$

Where $\forall k, j \in [1..n], w_{k,j} = \frac{e^{-||\mu_k - \mu_j||^2}}{\sum_{p,q \neq p} e^{-||\mu_p - \mu_q||^2}}$ and $w_k = \sum_{j \neq k} w_{k,j}$, such that $\sum_{k=1}^n w_k = 1$. The scalar w_k quantifies whether the positive sample $\bar{x}_k$ is "hard" (i.e. close to other samples in the batch), while $w_{k,j}$ quantifies whether the negative sample $\bar{x}_j$ is "hard" (i.e. close to the positive sample $\bar{x}_k$). Alignment is enforced through the first term of the gradient ($-\mu_{\bar{x}_k}$, aligning all views in the same direction) and uniformity through the second term $(\mu_{\bar{x}_j})_{j \neq k}$.

---

[2]By Jensen's inequality $||\mu_{\bar{x}}|| \leq \mathbb{E}_{\mathcal{A}(x|\bar{x})}||f(x)|| = 1$ with equality iff f is constant on supp $\mathcal{A}(\cdot|\bar{x})$.

Consequently, there is neither negative-negative coupling (as in AlignUnif (Wang & Isola, 2020)) nor negative-positive coupling (as in InfoNCE (Poole et al., 2019; Oord et al., 2019)) because the scaling factors do not depend on the instance-discrimination task difficulty, but rather on the relative positions between centroids. Importantly, the gradients never vanish since $\sum_{k=1}^n w_k = 1$. Thus, our loss indeed solves the NPC problem using an elegant and simple form.

3.2. Intra-class connectivity hypothesis

Most recent theories about CL (Wang et al., 2022; HaoChen et al., 2021) make the hypothesis that samples from the same semantic class have overlapping augmented views, to provide guarantees on the downstream task when optimizing InfoNCE (Chen et al., 2020a) or Spectral Contrastive loss (HaoChen et al., 2021). This assumption, known as intra-class connectivity hypothesis, is very strong and only relies on the augmentation distribution $\mathcal{A}$. In particular, augmentations should not be "too weak", so that all intra-class samples are connected among them, and at the same time not "too strong", to prevent connections between inter-class samples and thus preserve the semantic information. Here, we prove that we can relax this hypothesis if we can provide a kernel (viewed as a similarity function between original samples $\bar{x}$) that is "good enough" to relate intra-class samples not connected by the augmentations (see Fig. 1). In practice, we show that generative models (viewed as feature extractor) or auxiliary information can define such kernel. We first recall the definition of the augmentation graph (Wang et al., 2022), and intra-class connectivity hypothesis before presenting our main theorems. For simplicity, we assume that the set of images $\bar{\mathcal{X}}$ is finite (similarly to (Wang et al., 2022; HaoChen et al., 2021)). Our bounds and theoretical guarantees will never depend on the cardinality $|\bar{\mathcal{X}}|$.

Definition 3.3. (Augmentation graph (HaoChen et al., 2021; Wang et al., 2022)) Given a set of original images $\bar{\mathcal{X}}$, we define the augmentation graph $G_{\mathcal{A}}(V, E)$ for an augmentation distribution $\mathcal{A}$ through 1) a set of vertices $V = \bar{\mathcal{X}}$ and 2) a set of edges E such that $(\bar{x}, \bar{x}') = e \in E$ if the two original images $\bar{x}, \bar{x}'$ can be transformed into the same augmented image through $\mathcal{A}$, i.e supp $\mathcal{A}(\cdot|\bar{x}) \cap$ supp $\mathcal{A}(\cdot|\bar{x}') \neq \emptyset$.

Previous analysis in CL makes the hypothesis that there exists an optimal (accessible) augmentation module $\mathcal{A}^*$ that fulfills:

Previous Assumption 1. (Intra-class connectivity (Wang et al., 2022)) For a given downstream classification task $\mathcal{D} = \bar{\mathcal{X}} \times \mathcal{Y} \quad \forall y \in \mathcal{Y}$, the augmentation subgraph, $G_y \subset G_{\mathcal{A}^*}$ containing images only from class y, is connected.

Under this hypothesis, Decoupled Uniformity loss can tightly bound the downstream supervised risk without additional terms depending on batch size (*i.e.,* number of negative samples) **and** for a bigger class of encoders than pre-

vious works (not restricted to L-smooth functions (Wang et al., 2022)), as shown in Theorem 1.

Definition 3.4. (Weak-aligned encoder) An encoder $f \in \mathcal{F}$ is ϵ'-weak ($\epsilon' \geq 0$) aligned on $\mathcal{A}$ if $||f(x) - f(x')|| \leq \epsilon'$ $\quad \forall \bar{x} \in \bar{\mathcal{X}}, \forall x, x' \stackrel{i.i.d.}{\sim} \mathcal{A}(\cdot|\bar{x})$

Theorem 1. (Guarantees with $\mathcal{A}^*$) Given an optimal augmentation module $\mathcal{A}^*$, for any ϵ-weak aligned encoder $f \in \mathcal{F}$ we have: $\mathcal{L}_{unif}^{de}(f) \leq \mathcal{L}_{sup}(f) \leq 8D\epsilon + \mathcal{L}_{unif}^{de}(f)$ where D is the maximum diameter of all intra-class graphs G_y ($y \in \mathcal{Y}$). Proof in Appendix E.6.

In practice, the diameter D can be controlled by a small constant (*e.g.,* 4 in (Wang et al., 2022)) but it remains specific to the dataset at hand. In the next section, we study the case when $\mathcal{A}^*$ is not accessible or very hard to find.

3.3. Reconnect the disconnected: extending the augmentation graph with kernel

Having access to optimal augmentations is a strong assumption and, for many real-world applications (Saunshi et al., 2022), it may not be accessible. If we only have weak augmentations (*e.g.,* supp $\mathcal{A}(\cdot|\bar{x}) \subsetneq$ supp $\mathcal{A}^*(\cdot|\bar{x})$ for any $\bar{x}$), then some intra-class points might not be connected and we would need to reconnect them to ensure good downstream accuracy (see Theorem 7 in Appendix C.2). Augmentations are intuitive and they have been hand-crafted for decades by using human perception (*e.g.,* a rotated chair remains a chair and a gray-scale dog is still a dog). However, we may know other *prior information* about objects that are difficult to transfer through invariance to augmentations (*e.g.,* chairs should have 4 legs). This prior information can be either given as image attributes (*e.g.,* age or sex of a person, color of a bird, etc.) or, in an unsupervised setting, directly learnt through a generative model (*e.g.,* GAN or VAE). Now, we ask: how can we integrate this information inside a contrastive framework to reconnect intra-class images that are actually disconnected in $G_{\mathcal{A}}$? We rely on conditional mean embedding theory and use a kernel defined on the prior representation/information. This allows us to estimate a better configuration of the centroids in the representation space, with respect to the downstream task, and, ultimately, provide theoretical guarantees on the classification risk.

3.3.1. ϵ-KERNEL GRAPH

Definition 3.5. (RKHS on $\bar{\mathcal{X}}$) We define the RKHS $(\mathcal{H}_{\bar{\mathcal{X}}}, K_{\bar{\mathcal{X}}})$ on $\bar{\mathcal{X}}$ associated with a kernel $K_{\bar{\mathcal{X}}}$.

Example. If we work with large natural images, assuming that we know a prior $z(\bar{x})$ about our images (*e.g.,* given by a generative model), we can compute $K_{\bar{\mathcal{X}}}$ using z through $K_{\bar{\mathcal{X}}}(\bar{x}, \bar{x}') = \tilde{K}(z(\bar{x}), z(\bar{x}'))$ where $\tilde{K}$ is a standard kernel (*e.g.,* Gaussian or Cosine).

To link kernel theory with the previous augmentation graph, we need to define a *kernel graph* that connects images with high similarity in the kernel space.

Definition 3.6. (ϵ-Kernel graph) Let $\epsilon > 0$. We define the ϵ-kernel graph $G_{K_{\bar{\mathcal{X}}}}^{\epsilon}(V, E_K)$ for the kernel $K_{\bar{\mathcal{X}}}$ on $\bar{\mathcal{X}}$ through 1) a set of vertices $V = \bar{\mathcal{X}}$ and 2) a set of edges $E_{K_{\bar{\mathcal{X}}}}$ such that $e \in E_{K_{\bar{\mathcal{X}}}}$ between $\bar{x}, \bar{x}' \in \bar{\mathcal{X}}$ iff $\max(K_{\bar{\mathcal{X}}}(\bar{x}, \bar{x}), K_{\bar{\mathcal{X}}}(\bar{x}', \bar{x}')) - K_{\bar{\mathcal{X}}}(\bar{x}, \bar{x}') \leq \epsilon$.

The condition $\max(K_{\bar{\mathcal{X}}}(\bar{x}, \bar{x}), K_{\bar{\mathcal{X}}}(\bar{x}', \bar{x}')) - K_{\bar{\mathcal{X}}}(\bar{x}, \bar{x}') \leq \epsilon$ implies that $d_{K_{\bar{\mathcal{X}}}}(\bar{x}, \bar{x}') \leq 2\epsilon$ where $d_{K_{\bar{\mathcal{X}}}}(\bar{x}, \bar{x}') = K_{\bar{\mathcal{X}}}(\bar{x}, \bar{x}) + K_{\bar{\mathcal{X}}}(\bar{x}', \bar{x}') - 2K_{\bar{\mathcal{X}}}(\bar{x}, \bar{x}')$ is the kernel distance. For kernels with constant norm (*e.g.,* the standard Gaussian, Cosine or Laplacian kernel), it is in fact an equivalence. It means that we connect two original points in the kernel graph if they have small distance in the kernel space. We give now our main assumption to derive a better estimator of the centroid $\mu_{\bar{x}}$ in the insufficient augmentation regime.

Assumption 1. (Extended intra-class connectivity) For a given task $\mathcal{D} = \bar{\mathcal{X}} \times \mathcal{Y}$, the extended graph $\tilde{G} = G_{\mathcal{A}} \cup G_{K_{\bar{\mathcal{X}}}}^{\epsilon} = (V, E \cup E_{K_{\bar{\mathcal{X}}}})$ (union between augmentation graph and ϵ-kernel graph) is class-connected for all $y \in \mathcal{Y}$.

This assumption is notably weaker than Previous Assumption 1 w.r.t augmentation distribution $\mathcal{A}$. Here, we do not need to find the optimal distribution of augmentations $\mathcal{A}^*$, as long as we have a kernel $K_{\bar{\mathcal{X}}}$ such that disconnected points in the augmentation graph are connected in the ϵ-kernel graph. If K is not well adapted to the data-set (i.e it gives very low values for intra-class points), then ϵ needs to be large to re-connect these points and, as shown in Appendix A.1, the classification error will be high. In practice, this means that we need to tune the hyper-parameter of the kernel (e.g., σ for a RBF kernel) so that all intra-class points are reconnected with a small ϵ. This extra computation allows our framework to improve the final representation even for inadequate augmentations, as shown in Table 6.

3.3.2. CONDITIONAL MEAN EMBEDDING

Decoupled Uniformity loss includes no kernel in its raw form. It only depends on centroids $\mu_{\bar{x}} = \mathbb{E}_{\mathcal{A}(x|\bar{x})} f(x)$. Here, we show that another consistent estimator of these centroids can be defined, using the previous kernel $K_{\bar{\mathcal{X}}}$. To show it, we **fix** an encoder $f \in \mathcal{F}$ and require the following technical assumption in order to apply conditional mean embedding theory (Song et al., 2013; Klebanov et al., 2020).

Assumption 2. (Expressivity of $K_{\bar{\mathcal{X}}}$) The (unique) RKHS $(\mathcal{H}_f, K_f)$ defined on $\mathcal{X}$ with kernel $K_f = \langle f(\cdot), f(\cdot) \rangle_{\mathbb{R}^d}$ fulfills $\forall g \in \mathcal{H}_f, \mathbb{E}_{\mathcal{A}(x|\cdot)} g(x) \in \mathcal{H}_{\bar{\mathcal{X}}}$

Theorem 2. (Centroid estimation) Let $(x_i, \bar{x}_i)_{i \in [1..n]} \stackrel{iid}{\sim}$

$\mathcal{A}(x, \bar{x})$. Assuming 2, a consistent estimator of $\mu_{\bar{x}}$ is:

$$\forall \bar{x} \in \bar{\mathcal{X}}, \hat{\mu}_{\bar{x}} = \sum_{i=1}^{n} \alpha_i(\bar{x}) f(x_i) \quad (3)$$

where $\alpha_i(\bar{x}) = \sum_{j=1}^{n} [(K_n + n\lambda \mathbf{I}_n)^{-1}]_{ij} K_{\bar{\mathcal{X}}}(\bar{x}_j, \bar{x})$ and $K_n = [K_{\bar{\mathcal{X}}}(\bar{x}_i, \bar{x}_j)]_{i,j \in [1..n]}$. It converges to $\mu_{\bar{x}}$ with the ℓ_2 norm at a rate $O(n^{-1/4})$ for $\lambda = O(n^{-1/2})$. Proof in Appendix E.7.

Intuition. This theorem states that we can use representations of images close to an anchor $\bar{x}$, according to our prior information, to accurately estimate $\mu_{\bar{x}}$. Consequently, if the prior is "good enough" to connect intra-class images disconnected in the augmentation graph (i.e. fulfills Assumption 1), then this estimator allows us to tightly control the classification risk. From this theorem, we naturally derive the empirical Kernel Decoupled Uniformity loss using the previous estimator.

Definition 3.7. (Empirical Kernel Decoupled Uniformity Loss) Let $(x_i, \bar{x}_i)_{i \in [1..n]} \overset{iid}{\sim} \mathcal{A}(x, \bar{x})$. Let $\hat{\mu}_{\bar{x}_j} = \sum_{i=1}^{n} \alpha_{i,j} f(x_i)$ with $\alpha_{i,j} = ((K_n + \lambda n \mathbf{I}_n)^{-1} K_n)_{ij}$, $\lambda = O(n^{-1/2})$ a regularization constant and $K_n = [K_{\bar{\mathcal{X}}}(\bar{x}_i, \bar{x}_j)]_{i,j \in [1..n]}$. We define the empirical Kernel Decoupled Uniformity loss as:

$$\hat{\mathcal{L}}_{unif}^{de}(f) \overset{def}{=} \log \frac{1}{n(n-1)} \sum_{i \neq j} \exp(-||\hat{\mu}_{\bar{x}_i} - \hat{\mu}_{\bar{x}_j}||^2) \quad (4)$$

Extension to multi-views. If we have V views $(x_i^{(v)})_{v \in [1..V]}$ for each $\bar{x}_i$, we can easily extend the previous estimator with $\hat{\mu}_{\bar{x}_j} = \frac{1}{V} \sum_{v=1}^{V} \hat{\mu}_{\bar{x}_j}^{(v)}$ where $\hat{\mu}_{\bar{x}_j}^{(v)} = \sum_{i=1}^{n} \alpha_{i,j} f(x_i^{(v)})$. In practice, for a fair comparison with current SOTA contrastive methods, we set $V = 2$ in our experiments (see Appendix A.6 for a thorough discussion).

The computational cost added is roughly $O(n^3)$ (to compute the inverse matrix of size $n \times n$) but it remains negligible compared to the back-propagation time using classical stochastic gradient descent. Importantly, the gradients associated to $\alpha_{i,j}$ are not computed.

3.3.3. A TIGHT BOUND ON THE CLASSIFICATION LOSS WITH WEAKER ASSUMPTIONS

We show here that $\hat{\mathcal{L}}_{unif}^{de}(f)$ can tightly bound the supervised classification risk for well-aligned encoders $f \in \mathcal{F}$.

Theorem 3. We assume 1 and 2 hold for a reproducible kernel $K_{\bar{\mathcal{X}}}$ and augmentation distribution $\mathcal{A}$. Let $(x_i, \bar{x}_i)_{i \in [1..n]} \overset{iid}{\sim} \mathcal{A}(x, \bar{x})$. For any ϵ'-weak aligned encoder $f \in \mathcal{F}$:

$$\hat{\mathcal{L}}_{unif}^{de}(f) - O\left(n^{-1/4}\right) \leq \mathcal{L}_{sup}(f) \leq \hat{\mathcal{L}}_{unif}^{de}(f)+ \quad (5)$$

$$4D(2\epsilon' + \beta_n(K_{\bar{\mathcal{X}}})\epsilon) + O\left(n^{-1/4}\right)$$

where $\beta_n(K_{\bar{\mathcal{X}}}) = (\frac{\lambda_{min}(K_n)}{\sqrt{n}} + \sqrt{n}\lambda)^{-1} = O(1)$ for $\lambda = O(n^{-1/2})$, $K_n = (K_{\bar{\mathcal{X}}}(\bar{x}_i, \bar{x}_j))_{i,j \in [1..n]}$ and D is the maximal diameter of all sub-graphs $\tilde{G}_y \subset \tilde{G}$ where $y \in \mathcal{Y}$. We noted $\lambda_{min}(K_n) > 0$ the minimal eigenvalue of K_n. Proof in Appendix E.8.

Interpretation. Theorem 3 gives tight bounds on the classification loss $\mathcal{L}_{sup}(f)$ with weaker assumptions than current work (Saunshi et al., 2019; Wang et al., 2022; HaoChen et al., 2021). We don't require perfect alignment for $f \in \mathcal{F}$ or L-smoothness and we don't have class collision term (even if the extended augmentation graph may contain edges between inter-class samples), contrarily to (Saunshi et al., 2019). Also, the estimation error does not depend on the number of views (which is low in practice))–as it was always the case in previous formulations (Wang et al., 2022; Saunshi et al., 2019; HaoChen et al., 2021) – but rather on the batch size n and the eigenvalues of the kernel matrix (controlling the variance of the centroid estimator (Grünewälder et al., 2012)) . Contrarily to CCLK (Tsai et al., 2022), we don't condition our representation to weak attributes but rather we provide better estimation of the conditional mean embedding conditionally to the original image. Eventually, our loss remains in an unconditional contrastive framework driven by the augmentations $\mathcal{A}$ and the prior $K_{\bar{\mathcal{X}}}$ on input images. Theorem 1 becomes a special case $\epsilon = 0$ and $\mathcal{A} = \mathcal{A}^*$ (i.e the augmentation graph is class-connected, a stronger assumption than 1). In Appendix A.1, we provide empirical evidence that better kernel quality (measured by k-NN accuracy in kernel graph) improves downstream accuracy, as theoretically expected by the theorem. It also provides a new way to select *a priori* a good kernel.

4. Experiments

We study two regimes with our framework. We first start by evaluating our new loss, Decoupled Uniformity, without prior knowledge in an unsupervised scenario on standard vision benchmarks. Then, we study Kernel Decoupled Uniformity on both natural and medical datasets when prior knowledge is accessible (see Appendix A.4 for kernel choice). In the unsupervised scenario, we show that we can leverage generative models representation to outperform current self-supervised models. In the weakly supervised setting, we demonstrate the superiority of our unconditional formulation when weak attributes are available. Implementation details are presented in Appendix D. Importantly, most generative models are already pre-trained and are used as is in our framework (no additional computation).

Decoupled Uniformity without prior. We empirically demonstrate the benefits of removing the coupling between positives and negatives in the original uniformity term in InfoNCE loss (Wang & Isola, 2020) in Table 1 and 2. We

compare our approach with baseline InfoNCE (Oord et al., 2019) and DC (Yeh et al., 2022). We use the same setting as DC with batch size $n = 256$, initial learning rate 0.3 and temperature 0.07 for InfoNCE/DC losses.

Dataset	Network	$\mathcal{L}_{InfoNCE}$	$\mathcal{L}_{DC}$	$\mathcal{L}_{unif}^{de}$
CIFAR-10	ResNet18	$82.18_{\pm0.30}$	$84.87_{\pm0.27}$	$\mathbf{85.05}_{\pm0.37}$
CIFAR-100	ResNet18	$55.11_{\pm0.20}$	$58.27_{\pm0.34}$	$\mathbf{58.41}_{\pm0.05}$
ImageNet100	ResNet50	68.76	73.98	**77.18**

Table 1: Comparison of Decoupled Uniformity with InfoNCE/DC loss using SimCLR implementation under batch size $n = 256$. All models are trained for 400 epochs.

Generative models improve CL representation. We show that recent advances in generative modeling improve representations of contrastive models in Table 2 with our approach. Due to our limited computational resources, we study ImageNet100 (Tian et al., 2020) (100-class subset of ImageNet used in the literature (Tian et al., 2020; Chuang et al., 2020; Wang & Isola, 2020)) and we leverage BigBiGAN representation (Donahue & Simonyan, 2019) as prior. In particular, we use BigBiGAN pre-trained on ImageNet[3] to define a kernel $K_{GAN}(\bar{x}, \bar{x}') = K(z(\bar{x}), z(\bar{x}'))$ (with K an RBF kernel and $z(\cdot)$ BigBiGAN's encoder). We set $\lambda = \frac{0.01}{\sqrt{n}}$ for centroids estimation (see Appendix A.3). We demonstrate SOTA representation with this prior compared to all other contrastive and non-contrastive approaches.

Weakly supervised learning on natural images. In Table 3, we suppose that we have access to image attributes that correlate with the true semantic labels (e.g birds color/size for birds classification). We use three datasets: CUB-200-2011 (Welinder et al., 2010), ImageNet100 (Tian et al., 2020) and UTZappos (Yu & Grauman, 2014), following (Tsai et al., 2022). CUB-200-2011 contains 11788 images of 200 bird species with 312 binary attributes avail-

---
[3]Official model available here

Model	ImageNet100
SimCLR (Chen et al., 2020a)	68.76
BYOL (Grill et al., 2020)	72.26
CMC* (Tian et al., 2020)	73.58
DCL* (Chuang et al., 2020)	74.6
AlignUnif (Wang & Isola, 2020)	76.3
DC (Yeh et al., 2022)	73.98
SwAV (w/o multi-crop) (Caron et al., 2020)	73.5
BigBiGAN (Donahue & Simonyan, 2019)	72.0
Decoupled Unif	<u>77.18</u>
K_{GAN} Decoupled Unif	**78.02**
Supervised	$82.1_{\pm0.59}$

Table 2: Linear evaluation accuracy (%) on ImageNet100 using ResNet50 trained for 400 epochs with batch size $n = 256$ for all methods. *Results from paper.

Model	CUB	ImageNet100	UT-Zappos
SimCLR	17.48	65.30	84.08
BYOL	16.82	72.20	85.48
CosKernel CCLK (Tsai et al., 2022)	15.61	74.34	83.23
RBFKernel CCLK (Tsai et al., 2022)	30.49	77.24	84.65
CosKernel Decoupled Unif (ours)	27.77	**79.02**	**85.56**
RBFKernel Decoupled Unif (ours)	**32.87**	76.34	84.78

Table 3: If weak attributes are accessible (e.g birds color or size for CUB200), they can be leveraged as prior in our framework to improve the representation. CCLK is re-implemented using ResNet18 backbone.

able (encoding size, color, etc.). UTZappos contains 50025 images of shoes from several brands sub-categorized into 21 groups that we use as downstream classification labels. It comes with seven attributes. Finally, for ImageNet100 we follow (Tsai et al., 2022) and use the pre-trained CLIP (Radford et al., 2021) model (trained on pairs (text, image)) to extract 512-d features from images, considered as prior information. We use ResNet18 backbone for small-scale datasets (CUB and UTZappos) and ResNet50 for ImageNet100 (see Appendix D for more details). We compare our method with SOTA Siamese models (SimCLR and BYOL) and with CCLK, a conditional contrastive model that defines positive samples only according to the conditioning attributes. The proposed method outperforms all other models on the three datasets.

Model	Atelectasis	Cardiomegaly	Consolidation	Edema	Pleural Effusion
SimCLR	82.42	77.62	90.52	89.08	86.83
BYOL	83.04	81.54	90.98	90.18	85.99
MoCo-CXR*	75.8	73.7	77.1	86.7	85.0
GLoRIA	86.70	**86.39**	90.41	90.58	91.82
CCLK	86.31	83.67	92.45	91.59	91.23
K_{Gl} Dec. Unif (ours)	**86.92**	<u>85.88</u>	**93.03**	**92.39**	**91.93**
Supervised*	81.6	79.7	90.5	86.8	89.9

Table 4: AUC scores(%) under linear evaluation for discriminating 5 pathologies on CheXpert. ResNet18 backbone is trained for 400 epochs (batch size $n = 1024$) without labels on official CheXpert training set and results are reported on validation set.* Results from (Sowrirajan et al., 2021).

Medical imaging In order to evaluate our framework on another domain, we consider two challenging medical datasets. We study 1) bipolar disorder detection (BD), a challenging binary classification task, on brain MRI dataset BIOBD (Hozer et al., 2021) and 2) chest radiography interpretation, a 5-class classification task on CheXpert (Irvin et al., 2019). BIOBD contains 356 healthy controls (HC) and 306 patients with BD. We use BHB (Dufumier et al., 2021) as a large pre-training dataset containing 10k 3D images of healthy subjects. For brain MRI, we use VAE representation to define $K_{VAE}(\bar{x}, \bar{x}') = K(\mu(\bar{x}), \mu(\bar{x}'))$

where $\mu(\cdot)$ is the mean Gaussian distribution of $\bar{x}$ in the VAE latent space and K is a standard RBF kernel. For CheXpert, we use Gloria (Huang et al., 2021) representation[4], a multi-modal approach trained with (medical report, image) pairs to extract 2048-d features as weak annotations, on top of which we define our RBF kernel K_{Gl}. In Table 4 and 5, we show that our approach improve contrastive model in both unsupervised (BD) and weakly supervised (CheXpert) setting for medical imaging.

Model	BD vs HC
SimCLR (Chen et al., 2020a)	$60.46_{\pm1.23}$
BYOL (Grill et al., 2020)	$58.81_{\pm0.91}$
MoCo v2 (He et al., 2020)	$59.27_{\pm1.50}$
Model Genesis (Zhou et al., 2021)	$59.94_{\pm0.81}$
VAE (Kingma & Welling, 2013)	$52.86_{\pm1.24}$
K_{VAE} Decoupled Unif (ours)	$\mathbf{62.19}_{\pm1.58}$
Supervised	$67.42_{\pm0.31}$

Table 5: Linear evaluation AUC scores(%) using a 5-fold leave-site-out CV with DenseNet121 backbone.

Model	CIFAR-10			CIFAR-100		
	All	w/o Color	w/o Color and Crop	*All*	w/o Color	w/o Color and Crop
SimCLR	83.06	65.00	24.47	55.11	37.63	6.62
BYOL	84.71	81.45	50.17	53.15	49.59	27.9
Barlow Twins	81.61	53.97	47.52	52.27	28.52	24.17
VAE*	41.37	41.37	41.37	14.34	14.34	14.34
DCGAN*	66.71	66.71	66.71	26.17	26.17	26.17
K_{GAN} Dec. Unif	**85.85**	**82.0**	**69.19**	**58.42**	**54.17**	**35.98**

Table 6: When augmentation overlap hypothesis is not fulfilled, generative models provide a good kernel to connect intra-class points not connected by augmentations. *For VAE and DCGAN, no augmentations were used during training. All models are trained for 400 epochs under batch size $n = 256$ except BYOL and SimCLR trained under bigger batch size $n = 1024$.

Can we remove data augmentation from CL? As we saw in the visual domain, generative models can improve the representation of current CL framework. Theoretically, we saw that we can relax assumptions about the augmentation strategy we use in CL. It leads us to ask: is data augmentation still necessary in CL ?

We use standard benchmarking datasets (CIFAR-10, CIFAR-100) and we study the case where augmentations are too weak to connect all intra-class points. We compare to the baseline where all augmentations are used. We use a trained DCGAN (Radford et al., 2016) to define as before $K_{GAN}(\bar{x}, \bar{x}') \stackrel{\text{def}}{=} K(z(\bar{x}), z(\bar{x}'))$ where $z(\cdot)$ denotes the

[4]We use official pre-trained model available here

discriminator output of the penultimate layer[5].

In Table 6, we observe that our contrastive framework with DCGAN representation as prior is able to approach the performance of self-supervised models by applying only crop augmentations and flip. Additionally, when removing almost all augmentations (crop and color distortion), we approach the performance of the prior representations of the generative models. This is expected by our theory since we have an augmentation graph that is almost disjoint for all points and thus we only rely on the prior to reconnect them. This experiment shows that our method is less sensitive than all other SOTA self-supervised methods to the choice of the "optimal" augmentations.

Evading feature suppression with VAE. Previous investigations (Chen et al., 2021) have shown that a few easy-to-learn irrelevant features not removed by augmentations can prevent CL model from learning all semantic features inside images. We propose here a first solution to this issue by studying RandBits-CIFAR10 (Chen et al., 2021), a CIFAR-10 based dataset where k noisy bits are added and shared between views of the same image (see Appendix D.3). We train a ResNet18 on this dataset with SimCLR augmentations (Chen et al., 2020a) and increasing k. For Kernel Decoupled Uniformity, we use a β-VAE representation (ResNet18 backbone, $\beta = 1$, also trained on RandBits) to define K_{VAE} as before. In Table 7 we first show, as

Model	0 bits	5 bits	10 bits	20 bits
SimCLR (Chen et al., 2020a)	79.4	68.74	13.67	10.07
BYOL (Grill et al., 2020)	80.14	19.98	10.33	10.00
IFM-SimCLR (Robinson et al., 2021)	82.24	43.25	10.00	10.20
β-VAE ($\beta = 1$)	41.37	43.32	42.94	43.1
β-VAE ($\beta = 2$)	42.28	43.89	43.11	42.19
β-VAE ($\beta = 4$)	42.5	42.5	42.5	39.87
K_{VAE} Decoupled Unif (ours)	$\mathbf{82.74}_{\pm0.18}$	$\mathbf{68.75}_{\pm0.24}$	$\mathbf{68.42}_{\pm0.51}$	$\mathbf{68.58}_{\pm0.17}$

Table 7: Linear evaluation accuracy (%) on RandBits-CIFAR10 with ResNet18 trained for 200 epochs. For VAE, we use a ResNet18 backbone. Once trained, we use its representation to define the kernel K_{VAE}.

noted previously (Chen et al., 2021), that β-VAE is the only method insensitive to the number of added bits, but its representation quality remains low compared to other self-supervised approaches. All CL approaches fail for $k \geq 10$ bits. This can be explained by noticing that, as the number of bits k increases, the number of edges between intra-class images in the augmentation graph $G_{\mathcal{A}}$ decreases. For k bits, on average $N/2^k$ images share the same random bits ($N = 50000$ is the dataset size). So only these images can be connected in $G_{\mathcal{A}}$. For $k = 20$ bits, < 1 image share the same bits which means that they are almost all disconnected, and it explains why standard contrastive approaches fail. Same trend is observed for non-contrastive approaches (*e.g.*

[5]We prefered DCGAN over BigBiGAN in this experiment because we study smaller-scale datasets.

BYOL) with a degradation in performance even faster than SimCLR. Interestingly, encouraging a disentangled representation by imposing higher $\beta > 1$ in β-VAE does not help. Only our K_{VAE} Decoupled Uniformity loss obtains good scores, regardless of the number of bits.

5. Conclusion

In this work, we show that we can integrate prior information into CL to improve the final representation. In particular, we draw connections between kernel theory and CL to build our theoretical framework. We demonstrate tight bounds on downstream classification performance with weaker assumptions than previous works. Empirically, we show that generative models provide a good prior when augmentations are too weak or insufficient to remove easy-to-learn noisy features. We also show applications in medical imaging in both unsupervised and weakly supervised setting where our method outperforms all other models. Thanks to our theoretical framework, we hope that CL will benefit from the future progress in generative modelling and it will widen its field of application to challenging tasks, such as computer aided-diagnosis.

Acknowledgements

References

Azizi, S., Mustafa, B., Ryan, F., Beaver, Z., Freyberg, J., Deaton, J., Loh, A., Karthikesalingam, A., Kornblith, S., Chen, T., Natarajan, V., and Norouzi, M. Big Self-Supervised Models Advance Medical Image Classification. In *2021 IEEE/CVF International Conference on Computer Vision (ICCV)*, pp. 3458–3468. IEEE, 2021.

Bachman, P., Hjelm, R. D., and Buchwalter, W. Learning representations by maximizing mutual information across views. *Advances in neural information processing systems*, 32, 2019.

Becker, S. and Hinton, G. E. Self-organizing neural network that discovers surfaces in random-dot stereograms. *Nature*, 355(6356):161–163, 1992.

Borodachov, S. V., Hardin, D. P., and Saff, E. B. *Discrete energy on rectifiable sets*. Springer, 2019.

Bromley, J., Guyon, I., LeCun, Y., Säckinger, E., and Shah, R. Signature verification using a" siamese" time delay neural network. *Advances in neural information processing systems*, 6, 1993.

Caron, M., Misra, I., Mairal, J., Goyal, P., Bojanowski, P., and Joulin, A. Unsupervised learning of visual features by contrasting cluster assignments. *Advances in Neural Information Processing Systems*, 33:9912–9924, 2020.

Caron, M., Touvron, H., Misra, I., Jégou, H., Mairal, J., Bojanowski, P., and Joulin, A. Emerging properties in self-supervised vision transformers. In *Proceedings of the IEEE/CVF International Conference on Computer Vision*, pp. 9650–9660, 2021.

Chen, T., Kornblith, S., Norouzi, M., and Hinton, G. A Simple Framework for Contrastive Learning of Visual Representations. In *International Conference on Machine Learning*, pp. 1597–1607. PMLR, November 2020a. ISSN: 2640-3498.

Chen, T., Kornblith, S., Swersky, K., Norouzi, M., and Hinton, G. E. Big self-supervised models are strong semi-supervised learners. *Advances in neural information processing systems*, 33:22243–22255, 2020b.

Chen, T., Luo, C., and Li, L. Intriguing properties of contrastive losses. *Advances in Neural Information Processing Systems*, 34:11834–11845, 2021.

Chen, X., Fan, H., Girshick, R., and He, K. Improved baselines with momentum contrastive learning. *arXiv preprint arXiv:2003.04297*, 2020c.

Chuang, C.-Y., Robinson, J., Lin, Y.-C., Torralba, A., and Jegelka, S. Debiased contrastive learning. *Advances in neural information processing systems*, 33:8765–8775, 2020.

Coates, A., Ng, A., and Lee, H. An analysis of single-layer networks in unsupervised feature learning. In *Proceedings of the fourteenth international conference on artificial intelligence and statistics*, pp. 215–223. JMLR Workshop and Conference Proceedings, 2011.

Deng, J., Dong, W., Socher, R., Li, L.-J., Li, K., and Fei-Fei, L. Imagenet: A large-scale hierarchical image database. In *2009 IEEE conference on computer vision and pattern recognition*, pp. 248–255. Ieee, 2009.

Donahue, J. and Simonyan, K. Large scale adversarial representation learning. *Advances in Neural Information Processing Systems*, 32, 2019.

Donahue, J., Krähenbühl, P., and Darrell, T. Adversarial feature learning. *ICLR*, 2017.

Dufumier, B., Gori, P., Victor, J., Grigis, A., Wessa, M., Brambilla, P., Favre, P., Polosan, M., Mcdonald, C., Piguet, C. M., et al. Contrastive learning with continuous proxy meta-data for 3d mri classification. In *International Conference on Medical Image Computing and Computer-Assisted Intervention*, pp. 58–68. Springer, 2021.

Dumoulin, V., Belghazi, I., Poole, B., Mastropietro, O., Lamb, A., Arjovsky, M., and Courville, A. Adversarially learned inference. *ICLR*, 2017.

Dwibedi, D., Aytar, Y., Tompson, J., Sermanet, P., and Zisserman, A. With a little help from my friends: Nearest-neighbor contrastive learning of visual representations. In *Proceedings of the IEEE/CVF International Conference on Computer Vision*, pp. 9588–9597, 2021.

Foster, A., Pukdee, R., and Rainforth, T. Improving transformation invariance in contrastive representation learning. *ICLR*, 2021.

Goodfellow, I., Pouget-Abadie, J., Mirza, M., Xu, B., Warde-Farley, D., Ozair, S., Courville, A., and Bengio, Y. Generative adversarial nets. *Advances in neural information processing systems*, 27, 2014.

Graf, F., Hofer, C., Niethammer, M., and Kwitt, R. Dissecting supervised constrastive learning. In *International Conference on Machine Learning*, pp. 3821–3830. PMLR, 2021.

Grill, J.-B., Strub, F., Altché, F., Tallec, C., Richemond, P., Buchatskaya, E., Doersch, C., Avila Pires, B., Guo, Z., Gheshlaghi Azar, M., et al. Bootstrap your own latent-a new approach to self-supervised learning. *Advances in Neural Information Processing Systems*, 33:21271–21284, 2020.

Grünewälder, S., Lever, G., Baldassarre, L., Patterson, S., Gretton, A., and Pontil, M. Conditional mean embeddings as regressors-supplementary. *ICML*, 2012.

HaoChen, J. Z., Wei, C., Gaidon, A., and Ma, T. Provable guarantees for self-supervised deep learning with spectral contrastive loss. *Advances in Neural Information Processing Systems*, 34:5000–5011, 2021.

He, K., Zhang, X., Ren, S., and Sun, J. Deep residual learning for image recognition. In *Proceedings of the IEEE conference on computer vision and pattern recognition*, pp. 770–778, 2016.

He, K., Fan, H., Wu, Y., Xie, S., and Girshick, R. Momentum Contrast for Unsupervised Visual Representation Learning. In *CVPR*, pp. 9729–9738, 2020.

Hibar, D., Westlye, L. T., Doan, N. T., Jahanshad, N., Cheung, J., Ching, C. R., Versace, A., Bilderbeck, A., Uhlmann, A., Mwangi, B., et al. Cortical abnormalities in bipolar disorder: an mri analysis of 6503 individuals from the enigma bipolar disorder working group. *Molecular psychiatry*, 23(4):932–942, 2018.

Hozer, F., Sarrazin, S., Laidi, C., Favre, P., Pauling, M., Cannon, D., McDonald, C., Emsell, L., Mangin, J.-F., Duchesnay, E., et al. Lithium prevents grey matter atrophy in patients with bipolar disorder: an international multicenter study. *Psychological medicine*, 51(7):1201–1210, 2021.

Huang, G., Liu, Z., Van Der Maaten, L., and Weinberger, K. Q. Densely connected convolutional networks. In *Proceedings of the IEEE conference on computer vision and pattern recognition*, pp. 4700–4708, 2017.

Huang, S.-C., Shen, L., Lungren, M. P., and Yeung, S. Gloria: A multimodal global-local representation learning framework for label-efficient medical image recognition. In *Proceedings of the IEEE/CVF International Conference on Computer Vision*, pp. 3942–3951, 2021.

Irvin, J., Rajpurkar, P., Ko, M., Yu, Y., Ciurea-Ilcus, S., Chute, C., Marklund, H., Haghgoo, B., Ball, R., Shpanskaya, K., et al. Chexpert: A large chest radiograph dataset with uncertainty labels and expert comparison. In *Proceedings of the AAAI conference on artificial intelligence*, volume 33, pp. 590–597, 2019.

Jahanian, A., Puig, X., Tian, Y., and Isola, P. Generative models as a data source for multiview representation learning. *ICLR*, 2022.

Khosla, P., Teterwak, P., Wang, C., Sarna, A., Tian, Y., Isola, P., Maschinot, A., Liu, C., and Krishnan, D. Supervised contrastive learning. *Advances in Neural Information Processing Systems*, 33:18661–18673, 2020.

Kingma, D. P. and Welling, M. Auto-encoding variational bayes. *arXiv preprint arXiv:1312.6114*, 2013.

Klebanov, I., Schuster, I., and Sullivan, T. J. A rigorous theory of conditional mean embeddings. *SIAM Journal on Mathematics of Data Science*, 2(3):583–606, 2020.

Krizhevsky, A., Hinton, G., et al. Learning multiple layers of features from tiny images. 2009.

LeCun, Y. and Huang, F. J. Loss functions for discriminative training of energy-based models. In *International Workshop on Artificial Intelligence and Statistics*, pp. 206–213. PMLR, 2005.

Li, J., Zhou, P., Xiong, C., and Hoi, S. C. Prototypical contrastive learning of unsupervised representations. *ICLR*, 2021.

Oord, A. v. d., Li, Y., and Vinyals, O. Representation Learning with Contrastive Predictive Coding. *arXiv:1807.03748 [cs, stat]*, January 2019. URL http://arxiv.org/abs/1807.03748. arXiv: 1807.03748.

Poole, B., Ozair, S., Van Den Oord, A., Alemi, A., and Tucker, G. On variational bounds of mutual information. In *International Conference on Machine Learning*, pp. 5171–5180. PMLR, 2019.

Purushwalkam, S. and Gupta, A. Demystifying contrastive self-supervised learning: Invariances, augmentations and dataset biases. *Advances in Neural Information Processing Systems*, 33:3407–3418, 2020.

Radford, A., Metz, L., and Chintala, S. Unsupervised representation learning with deep convolutional generative adversarial networks. *ICLR*, 2016.

Radford, A., Kim, J. W., Hallacy, C., Ramesh, A., Goh, G., Agarwal, S., Sastry, G., Askell, A., Mishkin, P., Clark, J., et al. Learning transferable visual models from natural language supervision. In *International Conference on Machine Learning*, pp. 8748–8763. PMLR, 2021.

Robinson, J., Sun, L., Yu, K., Batmanghelich, K., Jegelka, S., and Sra, S. Can contrastive learning avoid shortcut solutions? *Advances in neural information processing systems*, 34:4974–4986, 2021.

Saunshi, N., Plevrakis, O., Arora, S., Khodak, M., and Khandeparkar, H. A theoretical analysis of contrastive unsupervised representation learning. In *International Conference on Machine Learning*, pp. 5628–5637. PMLR, 2019.

Saunshi, N., Ash, J., Goel, S., Misra, D., Zhang, C., Arora, S., Kakade, S., and Krishnamurthy, A. Understanding contrastive learning requires incorporating inductive biases. *ICML*, 2022.

Shah, H., Tamuly, K., Raghunathan, A., Jain, P., and Netrapalli, P. The pitfalls of simplicity bias in neural networks. *Advances in Neural Information Processing Systems*, 33: 9573–9585, 2020.

Song, L., Fukumizu, K., and Gretton, A. Kernel embeddings of conditional distributions: A unified kernel framework for nonparametric inference in graphical models. *IEEE Signal Processing Magazine*, 30(4):98–111, 2013.

Sowrirajan, H., Yang, J., Ng, A. Y., and Rajpurkar, P. Moco pretraining improves representation and transferability of chest x-ray models. In *Medical Imaging with Deep Learning*, pp. 728–744. PMLR, 2021.

Tian, Y., Krishnan, D., and Isola, P. Contrastive Multiview Coding. In Vedaldi, A., Bischof, H., Brox, T., and Frahm, J.-M. (eds.), *Computer Vision – ECCV 2020*, Lecture Notes in Computer Science, pp. 776–794, Cham, 2020. Springer International Publishing. ISBN 978-3-030-58621-8. doi: 10.1007/978-3-030-58621-8_45. tex.ids= tian_contrastive_2020 arXiv: 1906.05849.

Tsai, Y.-H. H., Li, T., Ma, M. Q., Zhao, H., Zhang, K., Morency, L.-P., and Salakhutdinov, R. Conditional contrastive learning with kernel. *ICLR*, 2022.

Wah, C., Branson, S., Welinder, P., Perona, P., and Belongie, S. The caltech-ucsd birds-200-2011 dataset. 2011.

Wang, T. and Isola, P. Understanding contrastive representation learning through alignment and uniformity on the hypersphere. In *International Conference on Machine Learning*, pp. 9929–9939. PMLR, 2020.

Wang, Y., Zhang, Q., Wang, Y., Yang, J., and Lin, Z. Chaos is a ladder: A new theoretical understanding of contrastive learning via augmentation overlap. *ICLR*, 2022.

Welinder, P., Branson, S., Mita, T., Wah, C., Schroff, F., Belongie, S., and Perona, P. Caltech-ucsd birds 200. 2010.

Yeh, C.-H., Hong, C.-Y., Hsu, Y.-C., Liu, T.-L., Chen, Y., and LeCun, Y. Decoupled contrastive learning. *ECCV*, 2022.

You, Y., Gitman, I., and Ginsburg, B. Large batch training of convolutional networks. *arXiv preprint arXiv:1708.03888*, 2017.

Yu, A. and Grauman, K. Fine-grained visual comparisons with local learning. In *Proceedings of the IEEE Conference on Computer Vision and Pattern Recognition*, pp. 192–199, 2014.

Zhai, X., Puigcerver, J., Kolesnikov, A., Ruyssen, P., Riquelme, C., Lucic, M., Djolonga, J., Pinto, A. S., Neumann, M., Dosovitskiy, A., et al. A large-scale study of representation learning with the visual task adaptation benchmark. *arXiv preprint arXiv:1910.04867*, 2019.

Zheng, M., Wang, F., You, S., Qian, C., Zhang, C., Wang, X., and Xu, C. Weakly supervised contrastive learning. In *Proceedings of the IEEE/CVF International Conference on Computer Vision*, pp. 10042–10051, 2021a.

Zheng, M., You, S., Wang, F., Qian, C., Zhang, C., Wang, X., and Xu, C. Ressl: Relational self-supervised learning with weak augmentation. *Advances in Neural Information Processing Systems*, 34, 2021b.

Zhou, Z., Sodha, V., Pang, J., Gotway, M. B., and Liang, J. Models genesis. *Medical image analysis*, 67:101840, 2021.

A. More empirical evidence

In this section, we provide additional empirical evidence to confirm several claims and arguments developed in the paper.

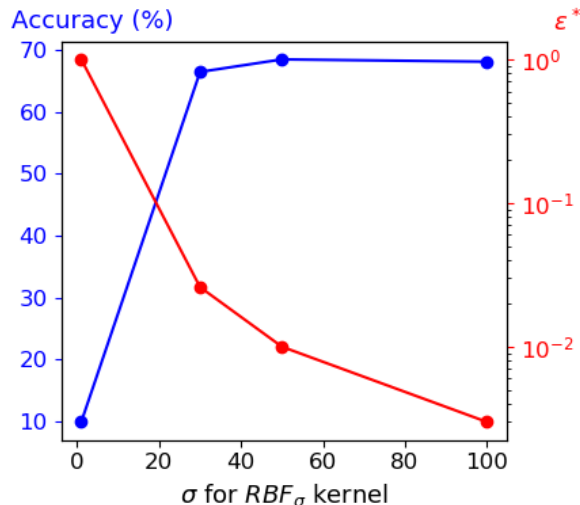## A.1. Measuring kernel quality and empirical verification of our theory

Figure 2: Empirical verification of our theory. The optimal ϵ^* to add 100 edges between intra-class images in ϵ-Kernel graph is inversely correlated with the downstream accuracy, as suggested by Theorem 3. We use $k = 20$ bits and an RBF kernel.
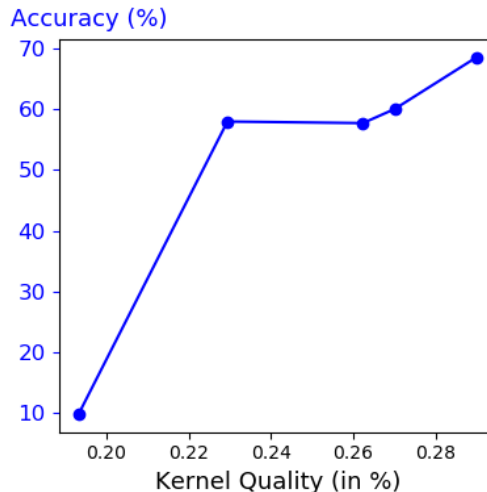
Figure 3: How can we select *a priori* a good kernel? Downstream accuracy on RandBits CIFAR-10 is highly correlated (Pearson's $r = 0.90$) with kernel quality measured as fraction of 10 nearest neighbors of the same CIFAR-10 class (from test set) in the kernel graph.

We provide empirical evidence confirming our theory (Theorem 3 in particular) along with a new way to quantify kernel quality with respect to a downstream task for a kernel K. We perform experiments on RandBits dataset (based on CIFAR-10) with $k = 20$ random bits (almost all points are disconnected in the augmentation graph) and SimCLR augmentations. For a given kernel K_σ defined by $K_\sigma(\bar{x}, \bar{x}') = RBF_\sigma(\mu(\bar{x}), \mu(\bar{x}'))$–where $\mu(\cdot)$ is the mean Gaussian distribution of $\bar{x}$ in VAE latent space trained on RandBits– we train Kernel Decoupled Uniformity with K_σ on RandBits. In Fig. 2, we vary σ and we report downstream accuracy (measured by linear evaluation) along with the optimal ϵ^* to add 100 intra-class edges in the ϵ-Kernel graph obtained with K_σ. The lower ϵ^*, the better the downstream accuracy, which is expected since the upper bound of supervised risk becomes tighter in Theorem 3. It gives a first empirical confirmation that ϵ tightly bounds the supervised risk on downstream task.

A new way to quantify kernel quality. Based on the concept of kernel graph, we measure the quality of a given kernel K using the nearest-neighbors of each image (a vertex in kernel graph). More precisely, K induces a distance d_K ($d_K(a, b) = K(a, a) + K(b, b) - 2K(a, b)$) that can be used to define nearest-neighbors in its kernel graph. We compute the fraction of these nearest neighbors that belong to the same class. In Fig. 3, we plot the downstream accuracy vs kernel quality using 10-nearest neighbors for various kernel K. They are obtained by using latent space of a VAE trained for an increasing number of epochs (2, 50, 100, 150 and 1000) and by setting $K(\bar{x}, \bar{x}') = RBF_\sigma(\mu(\bar{x}), \mu(\bar{x}'))$ as before (with $\sigma = 50$ fixed). It shows that this new measure of kernel quality is highly correlated with final downstream accuracy. Therefore, it can be used as a tool to compare *a priori* (without training) different kernels. One limitation of this metric is that it requires access to labels on the downstream task. Future work would consist in finding unsupervised properties of the kernel graph that correlates well with downstream accuracy (e.g. sparsity, clustering coefficient, etc.).

A.2. Influence of temperature and batch size for Decoupled Uniformity

InfoNCE is known to be sensitive to batch size and temperature to provide SOTA results. In our theoretical framework, we assumed that $f(x) \in \mathbb{S}^{d-1}$ but we can easily extend it to $f(x) \in \sqrt{t}\mathbb{S}^{d-1}$ where $t > 0$ is a hyper-parameter. It corresponds to write $\mathcal{L}_{unif}^{de}(f) = \mathbb{E}_{p(\bar{x})p(\bar{x}')} e^{-t||\mu_{\bar{x}} - \mu_{\bar{x}'}||^2}$. We show here that Decoupled Uniformity does not require very large batch

size (as it is the case for InfoNCE-based frameworks such as SimCLR) and produce good representations for $t \in [1, 5]$. In our default setting, we use $t = 2$ and batch size $n = 256$.

Datasets	$t = 0.1$	$t = 0.5$	$t = 1$	$t = 2$	$t = 5$	$t = 10$
CIFAR10	73.91	83.01	84.72	**85.82**	83.05	74.82
CIFAR100	39.16	51.33	55.91	**58.89**	56.70	48.29

Table 8: Linear evaluation accuracy (%) after training for 400 epochs with batch size $n = 256$ and varying temperature in Decoupled Uniformity loss with SimCLR augmentations. $t = 2$ gives overall the best results, similarly to the uniformity loss in (Wang & Isola, 2020)

Datasets	Loss	$n = 128$	$n = 512$	$n = 1024$	$n = 2048$
CIFAR10	InfoNCE	78.89	79.40	80.02	80.06
	Decoupled Unif	82.67	82.12	82.74	82.33
CIFAR100	InfoNCE	49.53	53.46	54.45	55.32
	Decoupled Unif	54.61	54.12	55.56	55.20

Table 9: Linear evaluation accuracy (%) after training for 200 epochs with a batch size n, ResNet18 backbone and latent dimension $d = 128$. Decoupled Uniformity is less sensitive to batch size than InfoNCE thanks to its decoupling between positives and negatives, similarly to (Yeh et al., 2022).

A.3. Importance of regularization λ in centroid estimation

Kernel Decoupled Uniformity introduces an additional hyper-parameter λ for centroids estimation, which should be such that $\lambda = O\left(\frac{1}{\sqrt{n}}\right)$ where n is the batch size to full-fill the hypothesis of Theorem 3. We have cross-validated this hyper-parameter λ on RandBits CIFAR-10 with $k = 10$ bits and we show in Table 10 that $\lambda = \frac{0.01}{\sqrt{n}}$ yields the best results. We have fixed this value for all our experiments in this study.

$\sqrt{256} \times \lambda$	$\sigma = 30$	$\sigma = 50$
0.001	10.25	60.75
0.01	**67.21**	**68.42**
0.1	59.09	58.13
1	50.49	60.75

Table 10: Importance of λ in centroids estimation with Kernel Decoupled Uniformity. We report linear evaluation accuracy after training on RandBits-CIFAR10 (10 bits) with ResNet18 for 200 epochs using RBFKernel(σ) and batch size $n = 256$.

A.4. Kernel choice

ImageNet100 with BigBiGAN. We cross-validate both RBF and Cosine kernel on top of BigBiGAN's encoder for Kernel Decoupled Uniformity. According to Table 11, we set $\sigma = 100$ with RBF for the experiments on ImageNet100.

Kernel	$\sigma = 1$	$\sigma = 10$	$\sigma = 100$	$\sigma = 150$	Cosine
ResNet50	73.36	72.6	**74.7**	74.38	73.88

Table 11: Linear evaluation accuracy(%) after training Kernel Decouped Uniformity on ImageNet-100 for 200 epochs with BigBiGAN's representation as prior. We study RBF Kernel with bandwidth σ or Cosine Kernel on top of BigBiGAN's encoder.

RandBits experiment. In our experiments on RandBits, we used RBF Kernel in Decoupled Uniformity but other kernels can be considered. Here, we have compared our approach with a cosine kernel on Randbits with $k = 10$ and $k = 20$ bits. There is no hyper-parameter to tune with cosine. From Table 12, we see that cosine gives comparable results for $k = 10$ bits with RBF but it is not appropriate for $k = 20$ bits.

Kernel	10 bits	20 bits
RBFKernel($\sigma = 1$)	$66.25_{\pm 0.17}$	$9.91_{\pm 0.13}$
RBFKernel($\sigma = 30$)	$67.21_{\pm 0.29}$	$66.46_{\pm 0.19}$
RBFKernel($\sigma = 50$)	$\mathbf{68.42_{\pm 0.51}}$	$\mathbf{68.58_{\pm 0.17}}$
CosineKernel	$66.56_{\pm 0.45}$	$9.68_{\pm 0.18}$

Table 12: Linear evaluation accuracy after training on RandBits-CIFAR10 with ResNet18 for 200 epochs. RBF and Cosine kernels are evaluated.

Weakly supervised learning. In this case, we compared our approach with CCLK (Tsai et al., 2022), also based on kernel. For this comparison, we use two kernels (RBF and Cosine) on all 3 benchmarking dataset (CUB200, ImageNet100 and UTZappos). We fixed $\sigma = 20$, $\sigma = 10$, $\sigma = 100$ respectively for CUB200, ImageNet100 and UTZappos using RBF Kernel, cross-validated in $\{1, 10, 20, 50, 100\}$ using linear evaluation on downstream task.

Medical imaging. For the experiments on CheXpert, we used an RBF Kernel on top of GloRIA's representation and we fixed $\sigma = 10$. For the pre-training on BHB using VAE representation as prior, we set $\sigma = 100$.

A.5. Larger pre-trained generative model induces better prior

We argue that using larger datasets (*e.g.,* ImageNet 1K) for pre-training larger generative models will improve the prior on smaller-scale datasets and improve even more the final representations with our method. We have tested this hypothesis on CIFAR-10 and BigBiGAN as prior, compared to DCGAN pre-trained on CIFAR-10 and the other approaches without prior.

Model	CIFAR-10
SimCLR (Chen et al., 2020a)	81.75
BYOL (Grill et al., 2020)	81.97
Decoupled Unif	85.82
K_{DCGAN} Decoupled Unif	85.85
$K_{BigBiGAN}$ Decoupled Unif	**86.86**

Table 13: We evaluate Kernel Decoupled Uniformity with BigBiGAN pre-trained on ImageNet as prior knowledge. We compare this approach with a shallow DCGAN pre-trained on CIFAR-10 as prior. We train ResNet18 on CIFAR10 for 400 epochs and we report linear evaluation accuracy. Pre-trained generative models on larger datasets improve the final representation.

A.6. Multi-view Contrastive Learning with Decoupled Uniformity

When the intra-class connectivity hypothesis is full-filled, we showed that Decoupled Uniformity loss can tightly bound the classification risk for well-aligned encoders (see Theorem 1). Under that hypothesis, we consider the standard empirical estimator of $\mu_{\bar{x}} \approx \sum_{v=1}^{V} f(x^{(v)})$ for V views. Using all SimCLR augmentations, we empirically verify that increasing V allows for: 1) a better estimate of $\mu_{\bar{x}}$ which implies a faster convergence and 2) better results on standard benchmarking vision datasets (CIFAR10, CIFAR100, STL10). We always use batch size $n = 256$ for all approaches with ResNet18 backbone for CIFAR10, CIFAR100 and STL10. For STL-10, we use both labelled and unlabelled training data to train our encoder. We report the results in Table 14.

Model	CIFAR-10		CIFAR-100		STL10	
	$e = 200$	$e = 400$	$e = 200$	$e = 400$	$e = 200$	$e = 400$
SimCLR(Chen et al., 2020a)	79.4	81.75	48.89	53.02	76.99	79.02
BYOL(Grill et al., 2020)	80.14	81.97	51.57	53.65	77.62	79.61
Decoupled Unif (2 views)	82.43	**85.82**	54.01	58.89	78.12	79.89
Decoupled Unif (4 views)	84.99	85.34	57.23	59.07	78.25	**80.47**
Decoupled Unif (8 views)	**86.50**	85.80	**59.63**	**59.74**	**79.82**	80.30

Table 14: A better approximation of centroids $\mu_{\bar{x}}$ (i.e. increasing number of views) when augmentation overlap hypothesis is (nearly) full-filled implies faster convergence. All models are pre-trained with batch size $n = 256$. We use ResNet18 backbone for CIFAR10, CIFAR100, STL10. We report linear evaluation accuracy (%) for a given number of epochs e.
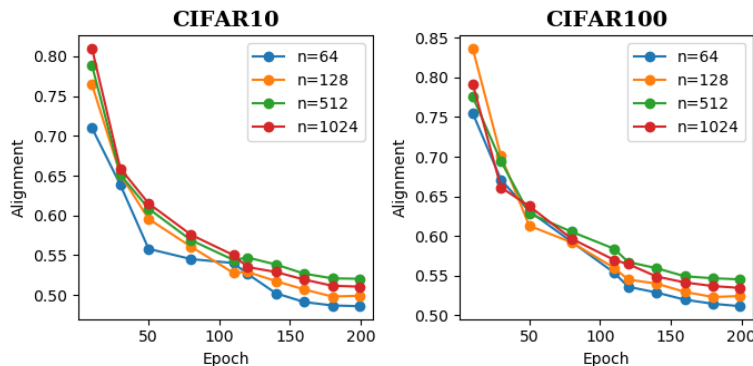

Figure 4: Alignment metric $\mathcal{L}_{align}$ computed on the validation set during optimization of Decoupled Uniformity loss with various batch sizes n and a fixed latent space dimension $d = 128$. We use 100 positive samples per image to compute $\mathcal{L}_{align}$.

A.7. Decoupled Uniformity optimizes alignment

We empirically show here that Decoupled Uniformity optimizes alignment, even in the regime when the batch size $n > d+1$, where d is the representation space dimension. We use CIFAR-10 and CIFAR-100 datasets and we optimize Decoupled Uniformity (without kernel) with all SimCLR augmentations with $d = 128$ and we vary the batch size n. We report the alignment metric defined in (Wang & Isola, 2020) as $\mathcal{L}_{align} = \mathbb{E}_{\mathcal{A}(x|\bar{x})\mathcal{A}(x'|\bar{x})p(\bar{x})}||f(x) - f(x')||^2$. In Fig. A.7, we notice that $\mathcal{L}_{align}$ is minimized as we optimize $\mathcal{L}_{unif}^{de}$ and we reach $\mathcal{L}_{align} \approx 0.50$ after 200 epochs, which is approximately the same result as in (Wang & Isola, 2020) by directly optimizing alignment and their uniformity term. In our case, alignment is implicit and we do not need to add it to our loss (avoiding the tuning of an additional hyper-parameter).

B. Geometrical considerations about Decoupled Uniformity

B.1. Asymptotical optimality

Theorem 4. (Optimality of Decoupled Uniformity) Given n points $(\bar{x}_i)_{i \in [1..n]}$ such that $n \leq d + 1$, any optimal encoder f^* minimizing $\hat{\mathcal{L}}_{unif}^{de}$ achieves a representation s.t.:

1. (Perfect uniformity) All centroids $(\mu_{\bar{x}_i})_{i \in [1..n]}$ make a regular simplex on the hyper-sphere $\mathbb{S}^{d-1}$

2. (Perfect alignment) f^* is perfectly aligned, i.e $\forall x, x' \sim \mathcal{A}(\cdot|\bar{x}_i), f^*(x) = f^*(x')$ for all $i \in [1..n]$.

Proof in Appendix E.3.

Contrary to (Wang & Isola, 2020), we are able to derive a geometrical characterization of the optimal representation for a finite batch size $n < \infty$ (*i.e.,* number of negatives), corresponding to a real-life scenario. Importantly, our uniformity term is distinct from the definition in (Wang & Isola, 2020) which is only defined for $n \to \infty$.

The assumption $n \leq d + 1$ is crucial to have the existence of a regular simplex on the hypersphere $\mathbb{S}^{d-1}$. In practice, this condition is not always full-filled (e.g SimCLR (Chen et al., 2020a) with $d = 128$ and $n = 4096$). Characterizing the optimal solution of $\mathcal{L}_{unif}^{de}$ for any $n > d + 1$ is still an open problem (Borodachov et al., 2019) but theoretical guarantees can be obtained in the limit case $n \to \infty$.

Theorem 5. (Asymptotical Optimality) When the number of samples is infinite $n \to \infty$, then for any perfectly aligned encoder $f \in \mathcal{F}$ that minimizes $\mathcal{L}_{unif}^{de}$, the centroids $\mu_{\bar{x}}$ for $\bar{x} \sim p(\bar{x})$ are uniformly distributed on the hypersphere $\mathbb{S}^{d-1}$. Proof in Appendix E.3.

Empirically, we observe that minimizers f of $\hat{\mathcal{L}}_{unif}^{de}$ remain well-aligned when $n > d + 1$ on real-world vision datasets (see Appendix A.7). Decoupled uniformity thus optimizes two properties that are nicely correlated with downstream classification performance (Wang & Isola, 2020)–that is alignment and uniformity between centroids. However, as noted in (Wang et al., 2022; Saunshi et al., 2022), optimizing these two properties is necessary but not sufficient to guarantee a good classification accuracy. In fact, the accuracy can be arbitrarily bad even for perfectly aligned and uniform encoders (Saunshi et al., 2022).

B.2. A metric learning point-of-view

In this section, we provide a geometrical understanding of Decoupled Uniformity loss from a metric learning point of view. In particular, we consider the Log-Sum-Exp (LSE) operator often used in CL as an approximation of the maximum.

We consider the finite-samples case with n original samples $(\bar{x}_i)_{i \in [1..n]} \overset{iid}{\sim} p(\bar{x})$ and V views $(x_i^{(v)})_{v \in [1..V]} \overset{iid}{\sim} \mathcal{A}(\cdot | \bar{x}_i)$ for each sample $\bar{x}_i$. We make an abuse of notations and set $\mu_i = \frac{1}{V} \sum_{v=1}^{V} f(x_i^{(v)})$. Then we have:

$$
\begin{aligned}
\hat{\mathcal{L}}_{unif}^{de} &= \log \frac{1}{n(n-1)} \sum_{i \neq j} \exp\left(-||\mu_i - \mu_j||^2\right) \\
&= \log \frac{1}{n(n-1)} \sum_{i \neq j} \exp\left(-s_i^+ - s_j^+ + 2s_{ij}^-\right)
\end{aligned}
\tag{6}
$$

where $s_i^+ = ||\mu_i||^2 = \frac{1}{V^2} \sum_{v,v'} s(x_i^{(v)}, x_i^{(v')})$, $s_{ij}^- = \frac{1}{V^2} \sum_{v,v'} s(x_i^{(v)}, x_j^{(v')})$ and $s(\cdot, \cdot) = \langle f(\cdot), f(\cdot) \rangle_2$ is viewed as a similarity measure.

From a metric learning point-of-view, we shall see that minimizing Eq. 6 is (almost) equivalent to looking for an encoder f such that the sum of similarities of all views from the same anchor (s_i^+ and s_j^+) are higher than the sum of similarities between views from different instances (s_{ij}^-):

$$
s_i^+ + s_j^+ > 2s_{ij}^- + \epsilon \quad \forall i \neq j
\tag{7}
$$

where ϵ is a margin that we suppose "very big" (see hereafter). Indeed, this inequality is equivalent to $-\epsilon > 2s_{ij}^- - s_i^+ - s_j^+$ for all $i \neq j$, which can be written as :

$$
\arg \min_{f} \max(-\epsilon, \{2s_{ij}^- - s_i^+ - s_j^+\}_{i,j \in [1..n], j \neq i})
$$

This can be transformed into an optimization problem using the LSE (log-sum-exp) approximation of the $\max$ operator:

$$
\arg \min_{f} \log \left(\exp(-\epsilon) + \sum_{i \neq j} \exp\left(-s_i^+ - s_j^+ + 2s_{ij}^-\right) \right)
$$

Thus, if we use an infinite margin ($\lim_{\epsilon \to \infty}$) we retrieve exactly our optimization problem with Decoupled Uniformity in Eq.6 (up to an additional constant depending on n).

C. Additional general guarantees on downstream classification

C.1. Optimal configuration of the supervised loss

In order to derive guarantees on a downstream classification task $\mathcal{D}$ when optimizing our unsupervised decoupled uniformity loss, we define a supervised loss that measures the risk on a downstream supervised task. We prove in the next section that the minimizers of this loss have the same geometry as the ones minimizing cross-entropy and SupCon (Khosla et al., 2020): a regular simplex on the hyper-sphere (Graf et al., 2021). More formally, we have:

Lemma 6. Let a downstream task $\mathcal{D}$ with C classes. We assume that $C \leq d + 1$ (*i.e.,* a big enough representation space), that all classes are balanced and the realizability of an encoder $f^* = \arg\min_{f \in \mathcal{F}} \mathcal{L}_{sup}(f)$ with $\mathcal{L}_{sup}(f) = \log \mathbb{E}_{y,y' \sim p(y)p(y')} e^{-||\mu_y - \mu_{y'}||^2}$, and $\mu_y = \mathbb{E}_{p(\bar{x}|y)} \mu_{\bar{x}}$. Then the optimal centroids $(\mu_y^*)_{y \in \mathcal{Y}}$ associated to f^* make a regular simplex on the hypersphere $\mathbb{S}^{d-1}$ and they are perfectly linearly separable, i.e $\min_{(w_y)_{y \in \mathcal{Y}} \in \mathbb{R}^d} \mathbb{E}_{(\bar{x},y) \sim \mathcal{D}} \mathbb{1}(w_y \cdot \mu_y^* < 0) = 0$. Proof in Appendix C.1

This property notably implies that we can realize 100% accuracy at optima with linear evaluation (taking the linear classifier $g(\bar{x}) = W^* f^*(\bar{x})$ with $W^* = (\mu_y^*)_{y \in \mathcal{Y}} \in \mathbb{R}^{C \times d}$).

C.2. General guarantees of Decoupled Uniformity

In its most general formulation, we tightly bound the previous supervised loss by Decoupled Uniformity loss $\mathcal{L}_{unif}^{de}$ depending on a variance term of the centroids $\mu_{\bar{x}}$ conditionally to the labels:

Theorem 7. (Guarantees for a given downstream task) For any $f \in \mathcal{F}$ and augmentation $\mathcal{A}$ we have:

$$\mathcal{L}_{unif}^{de}(f) \leq \mathcal{L}_{sup}(f) \leq 2 \sum_{j=1}^{d} \mathrm{Var}(\mu_{\bar{x}}^j | y) + \mathcal{L}_{unif}^{de}(f) \leq 4 \mathbb{E}_{p(\bar{x}|y)p(\bar{x}'|y)} ||\mu_{\bar{x}} - \mu_{\bar{x}'}|| + \mathcal{L}_{unif}^{de}(f) \tag{8}$$

where $\mathrm{Var}(\mu_{\bar{x}}^j | y) = \mathbb{E}_{p(\bar{x}|y)}(\mu_{\bar{x}}^j - \mathbb{E}_{p(\bar{x}'|y)} \mu_{\bar{x}'}^j)^2$, $y = \arg\max_{y' \in \mathcal{Y}} \mathrm{Var}(\mu_{\bar{x}}^j | y')$ and $\mu_{\bar{x}}^j$ is the j-th component of $\mu_{\bar{x}} = \mathbb{E}_{\mathcal{A}(x|\bar{x})} f(x)$. Proof in the next section.

Intuitively, it means that we will achieve good accuracy if all centroids $(\mu_{\bar{x}})_{\bar{x} \in \bar{\mathcal{X}}}$ for samples $\bar{x} \in \bar{\mathcal{X}}$ in the same class are not too far. This theorem is very general since we do not require the intra-class connectivity assumption on $\mathcal{A}$; so any $\mathcal{A} \subset \mathcal{A}^*$ can be used.

D. Experimental details

The code is accessible at this https URL. We provide a detailed pseudo-code of our algorithm as well as all experimental details to reproduce the experiments ran in the manuscript.

D.1. Pseudo-code

Algorithm 1 Pseudo-code for computing $\hat{\mathcal{L}}_{unif}^{de}$

Require: Batch of images $(\bar{x}_1, ..., \bar{x}_n) \in \bar{\mathcal{X}}$, augmentation distribution $\mathcal{A}$, temperature t, regularization λ for centroid estimation, kernel K
1: $K_n \leftarrow (K(\bar{x}_i, \bar{x}_j))_{i,j \in [1..n]}$ {Compute the kernel matrix}
2: $\alpha \leftarrow (K_n + n\lambda \mathbf{I}_n)^{-1} K_n$ {Compute weights for centroid estimation}
3: $x_i^{(1)}, ..., x_i^{(V)} \overset{iid}{\sim} \mathcal{A}(\cdot | \bar{x}_i)$ {Sample V views per image}
4: $F \leftarrow (\frac{1}{V} \sum_{v=1}^{V} f(x_i^{(v)}))_{i \in [1..n]}$ {Compute the averaged images representation}
5: $\hat{\mu} \leftarrow \alpha F$ {Centroid estimation}
6: $\hat{\mathcal{L}}_{unif}^{de} \leftarrow \log \frac{1}{n(n-1)} \sum_{i \neq j} \exp(-t||\hat{\mu}_i - \hat{\mu}_j||^2)$ {Kernel Decoupled Uniformity loss }
output $\hat{\mathcal{L}}_{unif}^{de}$

D.2. Implementation in PyTorch

We provide a PyTorch implementation of previous pseudo-code in Algorithm 2. It is generalizable to any number of views and any kernel.

Algorithm 2 PyTorch implementation of $\hat{\mathcal{L}}_{unif}^{de}$ with kernel

---

```
1    # loader: generator of images
2    # n: batch size
3    # n_views: number of views
4    # d: latent space dimension
5    # f: encoder (with projection head)
6    # x: Tensor of shape [n, *]
7    # aug: augmentation module generating views
8    # K: kernel defined on image space
9    # lamb: hyper-parameter to estimate centroids
10   for x in loader:
11     alphas = (K(x, x) + n*lamb*torch.eye(n)).inverse() @ K(x, x)
12     x = aug(x, n_views) # shape=[n*n_views, *]
13     z = f(x).view([n, n_views, d]) # shape=[n, n_views, d]
14     mu = alphas.detach() @ z.mean(dim=1) # shape=[n, d]
15     loss = L(mu)
16     loss.backward()
17
18   def L(mu, t=2):
19     return torch.pdist(mu, p=2).pow(2).mul(-t).exp().mean().log()
20
```

D.3. Datasets

CIFAR (Krizhevsky et al., 2009)   We use the original training/test split with 50000 and 10000 images respectively of size 32×32.

STL-10 (Coates et al., 2011)   In unsupervised pre-training, we use all labelled+unlabelled images (105000 images) for training and the remaining 8000 for test with size 96×96. During linear evaluation, we only use the 5000 training labelled images for learning the weights.

CUB200-2011 (Wah et al., 2011)   This dataset is composed of 200 fine-grained bird species with 5994 training images and 5794 test images rescaled to 224×224.

UTZappos (Yu & Grauman, 2014)   This dataset is composed of images of shoes from zappos.com. In order to be comparable with the literature on weakly supervised learning, we follow (Tsai et al., 2022) and split it into 35017 training images and 15008 test images resized at 32×32.

ImageNet100 (Deng et al., 2009; Tian et al., 2020)   It is a subset of ImageNet containing 100 random classes and introduced in (Tian et al., 2020). It contains 126689 training images and 5000 testing images rescaled to 224×224. It notably allows a reasonable computational time since we runt all our experiments on a single server node with 4 V100 GPU.

BHB (Dufumier et al., 2021)   This dataset is composed of 10420 3D brain MRI images of size $121 \times 145 \times 121$ with $1.5mm^3$ spatial resolution. Only healthy subjects are included.

BIOBD (Hozer et al., 2021)   It is also a brain MRI dataset including 662 3D anatomical images and used for downstream classification. Each 3D volume has size $121 \times 145 \times 121$. It contains 306 patients with bipolar disorder vs 356 healthy controls and we aim at discriminating patients vs controls. It is particularly suited to investigate biomarkers discovery inside the brain (Hibar et al., 2018).

18

CheXpert (Irvin et al., 2019)   This dataset is composed of 224 316 chest radiogaphs of 65240 patients. Each radiograph comes with 14 medical obervations. We use the official training set for our experiments, following (Huang et al., 2021; Irvin et al., 2019) and we test the models on the hold-out official validation split containing radiographs from 200 patients. For linear evaluation on this dataset, we train 5 linear probes to discriminate 5 pathologies (as binary classification) using only the radiographs with "certain" labels.

RandBits-CIFAR10 (Chen et al., 2021).   We build a RandBits dataset based on CIFAR-10. For each image, we add a random integer i sampled in $[0, 2^k - 1]$ where $k \in \{0, 5, 10, 20\}$ is a controllable number of bits. To make i easy to learn, we take its binary representation (*e.g.,* $(10101)_2$ for $i = 21$) and repeat each binary value spatially to define k channels that are added to the original RGB channels in each CIFAR-10 image. Importantly, these channels will not be altered by augmentations, so they will be shared across views.

D.4. Contrastive models

Architecture.   For all small-scale vision datasets (CIFAR-10 (Krizhevsky et al., 2009), CIFAR-100 (Krizhevsky et al., 2009), STL-10 (Coates et al., 2011), CUB200-2011 (Wah et al., 2011) and UT-Zappos (Yu & Grauman, 2014)) and CheXpert, we used official ResNet18 (He et al., 2016) backbone where we replaced the first 7×7 convolutional kernel by a smaller 3×3 kernel and we removed the first max-pooling layer for CIFAR-10, CIFAR-100 and UTZappos. For ImageNet100, we used ResNet50 (He et al., 2016) for stronger baselines as it is common in the literature. For medical images on brain MRI datasets (BHB (Dufumier et al., 2021) and BIOBD(Hozer et al., 2021), we used DenseNet121 (Huang et al., 2017) as our default backbone encoder, following previous literature on these datasets (Dufumier et al., 2021). We use the official

Following (Chen et al., 2020a), for our framework we use the representation space after the last average pooling layer with 2048 dimensions to perform linear evaluation and we use a 2-layers MLP projection head with batch normalization between each layer for a final latent space with $d = n$ dimensions (n being the batch size, default $n = 256$).

Batch size.   We always use a default batch size 256 for all experiments on vision datasets and 64 for brain MRI datasets (considering the computational cost with 3D images and since it had little impact on the performance (Dufumier et al., 2021)).

Optimization.   We use SGD optimizer on small-scale vision datasets (CIFAR-10, CIFAR-100, STL-10, CUB200-2011, UT-Zappos) with a base learning rate $0.3 \times$ batch size$/256$ and a cosine scheduler. For ImageNet100, we use a LARS (You et al., 2017) optimizer with learning rate $0.02 \times \sqrt{\text{batch size}}$ and cosine scheduler. In Kernel Decoupled Uniformity loss, we set $\lambda = \frac{0.01}{\sqrt{\text{batch size}}}$ and $t = 2$. For SimCLR, we set the temperature to $\tau = 0.07$ for all datasets following (Yeh et al., 2022). Unless mentioned otherwise, we use 2 views for Decoupled Uniformity (both with and without kernel) and the computational cost remains comparable with standard contrastive models.

Training epochs.   By default, we train the models for 400 epochs, unless mentioned otherwise for all vision data-sets excepted CUB200-2011 and UTZappos where we train them for 1000 epochs, following (Tsai et al., 2022). For medical brain MRI dataset, we perform pre-training for 50 epochs, as in (Dufumier et al., 2021). As for CheXpert, we train all models for 400 epochs.

Augmentations.   We follow (Chen et al., 2020a) to define our full set of data augmentations for vision datasets including: *RandomResizedCrop* (uniform scale between 0.08 to 1), *RandomHorizontalFlip* and color distorsion (including color jittering and gray-scale). For medical brain MRI dataset, we use cutout covering 25% of the image in each direction ($1/4^3$ of the entire volume), following (Dufumier et al., 2021). For CheXpert, we follow (Azizi et al., 2021³) and we use *RandomResizedCrop* (uniform scale between 0.08 to 1), *RandomHorizontalFlip*, *RandomRotation* (up to 45 degrees) however we do not apply color jittering as we work with gray-scale images.

D.4.1. GENERATIVE MODELS AND GLORIA

Architecture.   For VAE, we use ResNet18 backbone with a completely symmetric decoder using nearest-neighbor interpolation for up-sampling. For DCGAN, we follow the architecture described in (Radford et al., 2016). We keep the original dimension for CIFAR-10 and CIFAR-100 datasets and we resize the images to 64×64 for STL-10. For BigBiGAN (Donahue & Simonyan, 2019), we use the ResNet50 pre-trained encoder available at `https://tfhub.dev/`

`deepmind/bigbigan-resnet50/1` with BN+CReLU features.

Training. For VAE, we use PyTorch-lightning pre-trained model for STL-10 [6] and we optimize VAE for CIFAR-10 and CIFAR-100 for 400 epochs using an initial learning rate 10^{-4} and SGD optimizer with a cosine scheduler. For RandBits experiments, the VAE is trained with the same setup as for CIFAR-10/100 on RandBits-CIFAR10. For DCGAN, we optimize it using Adam optimizer (following (Radford et al., 2016)) and base learning rate 2×10^{-4}. Importantly, all generative models are trained without data augmentation, providing a fair comparison with other methods.

GloRIA(Huang et al., 2021) GloRIA can encode both image and text through 2 different encoders. It is pre-trained on the official training set of CheXpert, as in our experiments. We use only GloRIA image's encoder (a ResNet18 in practice[7]) to obtain weak labels on CheXpert and we leverage this weak labels with Kernel Decoupled Uniformity loss. In practice, we use an RBF kernel as in our previous experiments.

D.4.2. LINEAR EVALUATION

For all experiments (ImageNet100 excepted), we perform linear evaluation by encoding the original training set (without augmentation) and by training a logistic regression on these features. We cross-validate an ℓ_2 penalty term between $\{0, 1e-2, 1e-3, 1e-4, 1e-5\}$ for training this linear probe for 300 epochs with an initial learning rate 0.1 decayed by 0.1 at each plateau.

ImageNet100. On this dataset, we follow current practice (Yeh et al., 2022) and we train a linear classifier on top of the frozen encoder by applying the same augmentations as in pre-training. We train the classifier with SGD (momentum 0.9 and weight decay 0), batch size 512, initial learning rate 0.1 for 150 epochs (decayed by 0.1 at each plateau).

E. Proofs

E.1. Estimation error with the empirical Decoupled Uniformity loss

Property 1. $\hat{\mathcal{L}}_{unif}^{de}(f)$ fulfills $|\hat{\mathcal{L}}_{unif}^{de}(f) - \mathcal{L}_{unif}^{de}(f)| \leq O\left(\frac{1}{\sqrt{n}}\right)$ with a convergence in law.

PROOF. For any $x \in \mathcal{X}$, since $f(x) \in \mathbb{S}^{d-1}$, then $||\mu_{\bar{x}}|| = ||\mathbb{E}_{\mathcal{A}(x|\bar{x})} f(x)|| \leq \mathbb{E}_{\mathcal{A}(x|\bar{x})} ||f(x)|| = 1$. As a result, $e^{-||\mu_{\bar{x}} - \mu_{\bar{x}'}||^2} \in I \overset{\text{def}}{=} [e^{-4}, 1]$ for any $\bar{x}, \bar{x}' \in \bar{\mathcal{X}}$. Since log is k-Lipschitz on I then:

$$|\hat{\mathcal{L}}_{unif}^{de}(f) - \mathcal{L}_{unif}^{de}(f)| \leq k \left| \frac{1}{n(n-1)} \sum_{i \neq j} e^{-||\mu_{\bar{x}_i} - \mu_{\bar{x}_j}||^2} - \mathbb{E}_{p(\bar{x})p(\bar{x}')} e^{-||\mu_{\bar{x}} - \mu_{\bar{x}'}||^2} \right|$$

For a fixed $\bar{x} \in \bar{\mathcal{X}}$, let $g_n(\bar{x}) = \frac{1}{n} \sum_{i=1}^n e^{-||\mu_{\bar{x}} - \mu_{\bar{x}_i}||^2}$ and $g(\bar{x}) = \mathbb{E}_{p(\bar{x}')} e^{-||\mu_{\bar{x}} - \mu_{\bar{x}'}||^2}$. Since $(Z_i)_{i \in [1..n]} = \left(e^{-||\mu_{\bar{x}} - \mu_{\bar{X}_i}||^2} - g(\bar{x}) \right)_{i \in [1..n]}$ are iid with bounded support in $[-2, 2]$ and zero mean then by Berry–Esseen theorem we have $|g_n(\bar{x}) - g(\bar{x})| \leq O(\frac{1}{\sqrt{n}})$. Similarly, $(Z_i')_{i \in [1..n]} = \left(g_n(\bar{X}_i) - \mathbb{E}_{p(\bar{x})} g_n(\bar{x}) \right)$ are iid, bounded in $[-2, 2]$ and with zero mean. So $|\frac{1}{n} \sum_{i=1}^n g_n(\bar{x}_i) - \mathbb{E}_{p(\bar{x})} g_n(\bar{x})| \leq O(\frac{1}{\sqrt{n}})$ by Berry–Esseen theorem. Then we have:

$$|\hat{\mathcal{L}}_{unif}^{de}(f) - \mathcal{L}_{unif}^{de}(f)| \leq k |\frac{n}{(n-1)n} \sum_{i=1}^n g_n(\bar{x}_i) - \mathbb{E}_{p(\bar{x})} g(\bar{x})|$$

$$\leq 2k |\frac{1}{n} \sum_{i=1}^n g_n(\bar{x}_i) - \mathbb{E}_{p(\bar{x})} g_n(\bar{x}) + \mathbb{E}_{p(\bar{x})} g_n(\bar{x}) - \mathbb{E}_{p(\bar{x})} g(\bar{x})|$$

$$\leq O(\frac{1}{\sqrt{n}}) + O(\frac{1}{\sqrt{n}}) \leq O(\frac{1}{\sqrt{n}})$$

---

[6] `https://github.com/PyTorchLightning/pytorch-lightning`
[7] The official model is available here: `https://github.com/marshuang80/gloria`

E.2. Gradient analysis of Decoupled Uniformity

Proof. We start from the definition of our loss to derive the gradients: $\hat{\mathcal{L}}_{unif}^{de} = \log \frac{1}{n(n-1)} \sum_{j,i \neq j} \exp(-||\mu_i - \mu_j||^2)$ for a batch of n samples $(\bar{x}_i)_{i \in [1..n]}$ and we abuse the notation $\mu_i = \mu_{\bar{x}_i}$. Then we have:

$$
\begin{aligned}
\nabla_{\mu_k} \mathcal{L}_{unif}^{de} &= \frac{\frac{1}{n(n-1)} \sum_{j,i \neq j} \nabla_{\mu_k} \exp(-||\mu_i - \mu_j||^2)}{\frac{1}{n(n-1)} \sum_{j,i \neq j} \exp(-||\mu_i - \mu_j||^2)} \\
&= \frac{2 \sum_{j \neq k} e^{-||\mu_k - \mu_j||^2} (-2(\mu_k - \mu_j))}{\sum_{j,i \neq j} e^{-||\mu_i - \mu_j||^2}} \\
&= -4 \sum_{j \neq k} w_{k,j} (\mu_k - \mu_j) \\
&= -4 w_k \mu_k + 4 \sum_{j \neq k} w_{k,j} \mu_j
\end{aligned}
$$

We conclude that $\nabla_{z_k^{(v)}} \mathcal{L}_{unif}^{de} = -2 w_k \mu_k + 2 \sum_{j \neq k} w_{k,j} \mu_j$ by noticing that $\frac{\partial \mu_k}{\partial z_k^{(v)}} = \frac{1}{2}$ for two views since $\mu_k = \frac{1}{2}(z_k^{(1)} + z_k^{(2)})$. The extension to multiple views V is straightforward and do not change our main analysis.

E.3. Optimality of Decoupled Uniformity

Theorem 1. (Optimality of Decoupled Uniformity) Given n points $(\bar{x}_i)_{i \in [1..n]}$ such that $n \leq d + 1$, the optimal decoupled uniformity loss is reached when:

1. (Perfect uniformity) All centroids $(\mu_i)_{i \in [1..n]} = (\mu_{\bar{x}_i})_{i \in [1..n]}$ make a regular simplex on the hyper-sphere $\mathbb{S}^{d-1}$

2. (Perfect alignment) f is perfectly aligned, i.e $\forall x, x' \overset{iid}{\sim} \mathcal{A}(\cdot|\bar{x}_i), f(x) = f(x')$

PROOF. We will use Jensen's inequality and basic algebra to show these 2 properties. By triangular inequality, we have $||\mu_i|| = ||\mathbb{E}_{x \sim \mathcal{A}(.|\bar{x}_i)} f(x)|| \leq \mathbb{E}||f(x)|| = 1$ since we assume $f(x) \in \mathbb{S}^d$. So all (μ_i) are bounded by 1.

Let $\mu = (\mu_i)_{i \in [1..n]}$. We have:

$$
\begin{aligned}
\Gamma(\mu) := \sum_{i,j=1}^{n} ||\mu_i - \mu_j||^2 &= \sum_{i,j} ||\mu_i||^2 + ||\mu_j||^2 - 2\mu_i \cdot \mu_j \\
&\leq \sum_{i,j} (2 - 2\mu_i \cdot \mu_j) \\
&= 2n^2 - 2|| \sum_i \mu_i ||^2 \leq 2n^2
\end{aligned}
$$

with equality if and only if $\sum_{i=1}^n \mu_i = 0$ and $\forall i \in [1..n], ||\mu_i|| = 1$. By strict convexity of $u \to e^{-u}$, we have:

$$
\begin{aligned}
\sum_{i \neq j} \exp(-||\mu_i - \mu_j||^2) &\geq n(n-1) \exp\left(-\frac{\Gamma(\mu)}{n(n-1)}\right) \\
&\geq n(n-1) \exp\left(-\frac{2n}{n-1}\right)
\end{aligned}
$$

with equality if and only if all pairwise distance $||\mu_i - \mu_j||$ are equal (equality case in Jensen's inequality for strict convex function), $\sum_{i=1}^n \mu_i = 0$ and $||\mu_i|| = 1$. So all centroids must form a regular $n-1$-simplex inscribed on the hypersphere $\mathbb{S}^{d-1}$ centered at 0.

Finally, since $||\mu_i|| = 1$ then we have equality in the Jensen's inequality $||\mu_i|| = ||\mathbb{E}_{\mathcal{A}(x|\bar{x}_i)} f(x)|| \leq \mathbb{E}_{\mathcal{A}(x|\bar{x}_i)} ||f(x)|| = 1$. Since $|| \cdot ||$ is strictly convex on the hyper-sphere, then f must be constant on $\text{supp} \, \mathcal{A}(\cdot|\bar{x}_i)$, for all $\bar{x}_i$ so f must be perfectly aligned.

Theorem 5. (Asymptotical Optimality) When the number of samples is infinite $n \to \infty$, then for any perfectly aligned encoder $f \in \mathcal{F}$ that minimizes $\mathcal{L}_{unif}^d$, the centroids $\mu_{\bar{x}}$ for $\bar{x} \sim p(\bar{x})$ are uniformly distributed on the hypersphere $\mathbb{S}^{d-1}$.

PROOF. Let $f \in \mathcal{F}$ perfectly aligned. Then all centroids $\mu_{\bar{x}} = f(\bar{x})$ lie on the hypersphere $\mathbb{S}^{d-1}$ and we are optimizing:

$$\arg\min_f \mathcal{L}_{unif}^{de}(f) = \arg\min_f \mathbb{E}_{\bar{x},\bar{x}' \overset{iid}{\sim} p(\bar{x})} e^{-||f(\bar{x})-f(\bar{x}')||^2}$$

So a direct application of Proposition 1. in (Wang & Isola, 2020) shows that the uniform distribution on $\mathbb{S}^{d-1}$ is the unique solution to this problem and that all centroids are uniformly distributed on the hyper-sphere.

E.4. Optimality of the supervised loss

Lemma 6. Let a downstream task $\mathcal{D}$ with C classes. We assume that $C \leq d+1$ (*i.e.,* a big enough representation space), that all classes are balanced and the realizability of an encoder $f^* = \arg\min_{f \in \mathcal{F}} \mathcal{L}_{sup}(f)$ with $\mathcal{L}_{sup}(f) = \log \mathbb{E}_{y,y' \sim p(y)p(y')} e^{-||\mu_y - \mu_{y'}||^2}$, and $\mu_y = \mathbb{E}_{p(\bar{x}|y)} \mu_{\bar{x}}$. Then the optimal centroids $(\mu_y^*)_{y \in \mathcal{Y}}$ associated to f^* make a regular simplex on the hypersphere $\mathbb{S}^{d-1}$ and they are perfectly linearly separable, i.e $\min_{(w_y)_{y \in \mathcal{Y}} \in \mathbb{R}^d} \mathbb{E}_{(\bar{x},y) \sim \mathcal{D}} \mathbb{1}(w_y \cdot \mu_y^* < 0) = 0$.

PROOF. This proof is very similar to the one in Theorem 4. We first notice that all "labelled" centroids $\mu_y = \mathbb{E}_{p(\bar{x}|y)} \mu_{\bar{x}}$ are bounded by 1 ($||\mu_y|| \leq \mathbb{E}_{p(\bar{x}|y)} \mathbb{E}_{\mathcal{A}(x|\bar{x})} ||f(x)|| = 1$ by Jensen's inequality applied twice). Then, since all classes are balanced, we can re-write the supervised loss as:

$$\mathcal{L}_{sup}(f) = \log \frac{1}{C^2} \sum_{y,y'=1}^C e^{-||\mu_y - \mu_{y'}||^2}$$

We have:

$$\Gamma_{\mathcal{Y}}(\mu) := \sum_{y,y'=1}^C ||\mu_y - \mu_{y'}||^2 = \sum_{y,y'} ||\mu_y||^2 + ||\mu_{y'}||^2 - 2\mu_y \cdot \mu_{y'}$$

$$\leq \sum_{y,y'} (2 - 2\mu_y \cdot \mu_{y'})$$

$$= 2C^2 - 2|| \sum_y \mu_y||^2 \leq 2C^2$$

with equality if and only if $\sum_{y=1}^C \mu_y = 0$ and $\forall y \in [1..C], ||\mu_y|| = 1$. By strict convexity of $u \to e^{-u}$, we have:

$$\sum_{y \neq y'} \exp(-||\mu_y - \mu_{y'}||^2) \geq C(C-1) \exp\left(-\frac{\Gamma_{\mathcal{Y}}(\mu)}{C(C-1)}\right)$$

$$\geq C(C-1) \exp\left(-\frac{2C}{C-1}\right)$$

with equality if and only if all pairwise distance $||\mu_y - \mu_{y'}||$ are equal (equality case in Jensen's inequality for strict convex function), $\sum_{y=1}^C \mu_y = 0$ and $||\mu_y|| = 1$. So all centroids must form a regular $C-1$-simplex inscribed on the hypersphere $\mathbb{S}^{d-1}$ centered at 0. Furthermore, since $||\mu_y|| = 1$ then we have equality in the Jensen's inequality $||\mu_y|| = ||\mathbb{E}_{p(\bar{x}|y)\mathcal{A}(x|\bar{x})} f(x)|| \leq \mathbb{E}_{p(\bar{x}|y)\mathcal{A}(x|\bar{x})} ||f(x)|| = 1$ so f must by perfectly aligned for all samples belonging to the same class: $\forall \bar{x}, \bar{x}' \sim p(\cdot|y), f(\bar{x}) = f(\bar{x}')$.

E.5. Generalization bounds for the Decoupled Uniformity loss

Theorem 7. (Guarantees for a given downstream task) For any $f \in \mathcal{F}$ and augmentation distribution $\mathcal{A}$, we have:

$$\mathcal{L}_{unif}^{de}(f) \leq \mathcal{L}_{unif}^{sup}(f) \leq 2 \sum_{j=1}^d \mathrm{Var}(\mu_{\bar{x}}^j|y) + \mathcal{L}_{unif}^{de}(f) \leq 4\mathbb{E}_{p(\bar{x}|y)p(\bar{x}'|y)} ||\mu_{\bar{x}} - \mu_{\bar{x}'}|| + \mathcal{L}_{unif}^{de}(f) \tag{9}$$

where $\mathrm{Var}(\mu_{\bar{x}}^j|y) = \mathbb{E}_{p(\bar{x}|y)}(\mu_{\bar{x}}^j - \mathbb{E}_{p(\bar{x}'|y)}\mu_{\bar{x}'}^j)^2$ and $\mu_{\bar{x}}^j$ is the j-th component of $\mu_{\bar{x}} = \mathbb{E}_{\mathcal{A}(x|\bar{x})} f(x)$.

PROOF.

Lower bound. To derive the lower bound, we apply Jensen's inequality to convex function $u \to e^{-u}$:

$$
\begin{aligned}
\exp \mathcal{L}_{unif}^{de}(f) &= \mathbb{E}_{p(\bar{x})p(\bar{x}')} e^{-||\mu_{\bar{x}} - \mu_{\bar{x}'}||^2} \\
&= \mathbb{E}_{p(\bar{x}|y)p(\bar{x}'|y')p(y)p(y')} e^{-||\mu_{\bar{x}} - \mu_{\bar{x}'}||^2} \\
&\leq \mathbb{E}_{p(y)p(y')} \exp\left(-\mathbb{E}_{p(\bar{x}|y)p(\bar{x}'|y')}||\mu_{\bar{x}} - \mu_{\bar{x}'}||^2\right)
\end{aligned}
$$

Then, by Jensen's inequality applied to $||.||^2$:

$$
\begin{aligned}
\mathbb{E}_{p(\bar{x}|y)p(\bar{x}'|y')}||\mu_{\bar{x}} - \mu_{\bar{x}'}||^2 &\overset{(1)}{=} \mathbb{E}_{p(\bar{x}|y)}||\mu_{\bar{x}}||^2 + \mathbb{E}_{p(\bar{x}'|y')}||\mu_{\bar{x}'}||^2 - 2\mu_y \cdot \mu_{y'} \\
&\geq ||\mathbb{E}_{p(\bar{x}|y)}\mu_{\bar{x}}||^2 + ||\mathbb{E}_{p(\bar{x}'|y')}\mu_{\bar{x}'}||^2 - 2\mu_y \cdot \mu_{y'} \\
&\overset{(1)}{=} ||\mu_y - \mu_{y'}||^2
\end{aligned}
$$

(1) follows by definition of μ_y. So we can conclude:

$$
\exp \mathcal{L}_{unif}^{de}(f) \leq \mathbb{E}_{p(y)p(y')} \exp(-||\mu_y - \mu_{y'}||^2) = \exp \mathcal{L}_{unif}^{sup}
$$

Upper bound. For this bound, we will use the following equality (by definition of variance):

$$
\begin{aligned}
||\mathbb{E}_{p(\bar{x}|y)}\mu_{\bar{x}}||^2 &= ||\mathbb{E}_{p(\bar{x}|y)}\mu_{\bar{x}}||^2 - \mathbb{E}_{p(\bar{x}|y)}||\mu_{\bar{x}}||^2 + \mathbb{E}_{p(\bar{x}|y)}||\mu_{\bar{x}}||^2 \\
&= -\sum_{j=1}^{d} \text{Var}(\mu_{\bar{x}}^j|y) + \mathbb{E}_{p(\bar{x}|y)}||\mu_{\bar{x}}||^2
\end{aligned}
$$

So we start by expending:

$$
\begin{aligned}
||\mu_y - \mu_{y'}||^2 &= ||\mathbb{E}_{p(\bar{x}'|y')}\mu_{\bar{x}'}||^2 + ||\mathbb{E}_{p(\bar{x}|y)}\mu_{\bar{x}}||^2 - 2\mathbb{E}_{p(\bar{x}|y)p(\bar{x}'|y')}\mu_{\bar{x}} \cdot \mu_{\bar{x}'} \\
&= \mathbb{E}_{p(\bar{x}|y)}||\mu_{\bar{x}}||^2 + \mathbb{E}_{p(\bar{x}'|y')}||\mu_{\bar{x}'}||^2 - \left(\sum_{j=1}^{d} \text{Var}(\mu_{\bar{x}}^j|y) + \text{Var}(\mu_{\bar{x}'}^j|y)\right) - 2\mathbb{E}_{p(\bar{x}|y)p(\bar{x}'|y')}\mu_{\bar{x}} \cdot \mu_{\bar{x}'} \\
&= \mathbb{E}_{p(\bar{x}|y)p(\bar{x}'|y')}||\mu_{\bar{x}} - \mu_{\bar{x}'}||^2 - 2\left(\sum_{j=1}^{d} \text{Var}(\mu_{\bar{x}}^j|y)\right)
\end{aligned}
$$

So by applying again Jensen's inequality:

$$
\begin{aligned}
\exp \mathcal{L}_{unif}^{sup} = \mathbb{E}_{p(y)p(y')} \exp(-||\mu_y - \mu_{y'}||^2) &\leq \mathbb{E}_{p(y)p(y')} \exp\left(-\mathbb{E}_{p(\bar{x}|y)p(\bar{x}'|y')}||\mu_{\bar{x}} - \mu_{\bar{x}'}||^2 + 2\left(\sum_{j=1}^{d} \text{Var}(\mu_{\bar{x}}^j|y)\right)\right) \\
&\leq \exp 2\left(\sum_{j=1}^{d} \text{Var}(\mu_{\bar{x}}^j|y_m)\right) \mathbb{E}_{p(y)p(y')} \exp\left(-\mathbb{E}_{p(\bar{x}|y)p(\bar{x}'|y')}||\mu_{\bar{x}} - \mu_{\bar{x}'}||^2\right) \\
&= \exp 2\left(\sum_{j=1}^{d} \text{Var}(\mu_{\bar{x}}^j|y_m)\right) \exp \mathcal{L}_{unif}^{de}
\end{aligned}
$$

We set $y_m = \arg\max_{i,y \in [1..d] \times \mathcal{Y}} \text{Var}(\mu_{\bar{x}}^j|y)$ We conclude here by taking the $\log$ on the previous inequality.

Variance upper bound. Starting from the definition of conditional variance:

$$\sum_{j=1}^{d} \mathrm{Var}(\mu_{\bar{x}}^j | y_m) = \mathbb{E}_{p(\bar{x}|y_m)} ||\mu_{\bar{x}}||^2 - ||\mathbb{E}_{p(\bar{x}|y_m)}\mu_{\bar{x}}||^2$$

$$= \mathbb{E}_{p(\bar{x}|y_m)} \left((||\mu_{\bar{x}}|| - ||\mathbb{E}_{p(\bar{x}|y_m)}\mu_{\bar{x}}||)(||\mu_{\bar{x}}|| + ||\mathbb{E}_{p(\bar{x}|y_m)}\mu_{\bar{x}}||) \right)$$

$$\overset{(1)}{\leq} \mathbb{E}_{p(\bar{x}|y_m)} ||\mu_{\bar{x}} - \mathbb{E}_{p(\bar{x}'|y_m)}\mu_{\bar{x}'}||(||\mu_{\bar{x}}|| + ||\mathbb{E}_{p(\bar{x}|y_m)}\mu_{\bar{x}}||)$$

$$\overset{(2)}{\leq} 2\mathbb{E}_{p(\bar{x}|y_m)} ||\mu_{\bar{x}} - \mathbb{E}_{p(\bar{x}'|y_m)}\mu_{\bar{x}'}||$$

$$\overset{(3)}{\leq} 2\mathbb{E}_{p(\bar{x}|y_m)p(\bar{x}'|y_m)} ||\mu_{\bar{x}} - \mu_{\bar{x}'}||$$

(1) Follows from standard inequality $||a - b|| \geq |||a|| - ||b|||$ (from Cauchy-Schwarz). (2) follows from boundness of $||\mu_{\bar{x}}|| \leq 1$ and Jensen's inequality. (3) is again Jensen's inequality.

E.6. Generalization bound under intra-class connectivity assumption

Theorem 2. Assuming 1, then for any ϵ-weak aligned encoder $f \in \mathcal{F}$:

$$\mathcal{L}_{unif}^{de}(f) \leq \mathcal{L}_{unif}^{sup}(f) \leq 8D\epsilon + \mathcal{L}_{unif}^{d}(f) \tag{10}$$

Where D is the maximum diameter of all intra-class graphs G_y ($y \in \mathcal{Y}$).

PROOF. Let $y \in \mathcal{Y}$ and $\bar{x}, \bar{x}' \sim p(\bar{x}|y)p(\bar{x}'|y)$. By Assumption 1, it exists a path of length $p \leq D$ connecting $(\bar{x}, \bar{x}')$ in G_y. So it exists $(\bar{x}_i)_{i \in [1..p+1]} \in \bar{\mathcal{X}}$ and $(x_i)_{i \in [1..p]} \in \mathcal{X}$ s.t $\forall i \in [1..p], x_i \sim \mathcal{A}(x_i|\bar{x}_i) \cap \mathcal{A}(x_i|\bar{x}_{i+1})$, $\bar{x}_1 = \bar{x}$ and $\bar{x}_{p+1} = \bar{x}'$. Then:

$$||\mu_{\bar{x}} - \mu_{\bar{x}'}|| = ||\mu_{\bar{x}_1} - \mu_{\bar{x}_p}||$$

$$= ||\sum_{i=1}^{p} \mu_{\bar{x}_{i+1}} - \mu_{\bar{x}_i}||$$

$$\leq \sum_{i=1}^{p} ||\mu_{\bar{x}_{i+1}} - \mu_{\bar{x}_i}||$$

$$= \sum_{i=1}^{p} ||\mu_{\bar{x}_{i+1}} - f(x_i) + f(x_i) - \mu_{\bar{x}_i}||$$

$$\leq \sum_{i=1}^{p} ||\mu_{\bar{x}_{i+1}} - f(x_i)|| + ||f(x_i) - \mu_{\bar{x}_i}||$$

$$\overset{(1)}{\leq} \sum_{i=1}^{p} \mathbb{E}_{p(x|\bar{x}_{i+1})} ||f(x) - f(x_i)|| + \mathbb{E}_{p(x|\bar{x}_i)} ||f(x_i) - f(x)||$$

$$\overset{(2)}{\leq} \sum_{i=1}^{p} (\epsilon + \epsilon) = 2\epsilon p \leq 2\epsilon D$$

(1) follows from Jensen's inequality and by definition of $\mu_{\bar{x}}$. (2) follows because f is ϵ-weak aligned and $x_i \sim \mathcal{A}(x_i|\bar{x}_i) \cap \mathcal{A}(x_i|\bar{x}_{i+1})$.

So we have $||\mu_{\bar{x}} - \mu_{\bar{x}'}|| \leq 2\epsilon D$ and we can conclude by Theorem 7 (right inequality).

E.7. Conditional Mean Embedding Estimation

Theorem 3. (Conditional Mean Embedding estimation) Let $f \in \mathcal{F}$ fixed. We assume that $\forall g \in \mathcal{H}_{\mathcal{X}}, \mathbb{E}_{p(x|\cdot)}g(x) \in \mathcal{H}_{\bar{\mathcal{X}}}$. Let $\{(x_1, \bar{x}_1), ..., (x_n, \bar{x}_n)\}$ iid samples from $\mathcal{A}(x|\bar{x})p(\bar{x})$. Let $\Phi_n = [\phi(\bar{x}_1), ..., \phi(\bar{x}_n)]$ and $\Psi_f = [f(x_1), ..., f(x_n)]^T$. An

estimator of the conditional mean embedding is:

$$\forall \bar{x} \in \bar{\mathcal{X}}, \hat{\mu}_{\bar{x}} = \sum_{i=1}^{n} \alpha_i(\bar{x}) f(x_i) \tag{11}$$

where $\alpha_i(\bar{x}) = \sum_{j=1}^{n} [(\Phi_n^T \Phi_n + \lambda n \mathbf{I}_n)^{-1}]_{ij} \langle \phi(\bar{x}_j), \phi(\bar{x}) \rangle_{\mathcal{H}_{\bar{X}}}$. It converges to $\mu_{\bar{x}}$ with the ℓ_2 norm at a rate $O(n^{-1/4})$ for $\lambda = O(\frac{1}{\sqrt{n}})$.

PROOF. Let $m_{\bar{x}} = \mathbb{E}_{\mathcal{A}(x|\bar{x})} \langle f(x), f(\cdot) \rangle \in \mathcal{H}_{\mathcal{X}}$ be the conditional mean embedding operator. According to Theorem 6 in (Song et al., 2013) and the assumption $\forall g \in \mathcal{H}_{\mathcal{X}}, \mathbb{E}_{p(x|\cdot)} g(x) \in \mathcal{H}_{\bar{\mathcal{X}}}$, this estimator can be approximated by:

$$\hat{m}_{\bar{x}} = \sum_{i=1}^{n} \alpha_i(\bar{x}) \langle f(x_i), f(\cdot) \rangle$$

with α_i defined previously in the theorem. This estimator converges with RKHS norm to $m_{\bar{x}}$ at rate $O(\frac{1}{\sqrt{n\lambda}} + \lambda)$. So we need to link $m_{\bar{x}}, \hat{m}_{\bar{x}}$ with $\mu_{\bar{x}}, \hat{\mu}_{\bar{x}}$. We have:

$$
\begin{aligned}
\langle m_{\bar{x}}, \hat{m}_{\bar{x}} \rangle_{\mathcal{H}_{\mathcal{X}}} &= \left\langle \mathbb{E}_{p(x|\bar{x})} \langle f(x), f(\cdot) \rangle_{\mathbb{R}^d}, \sum_{i=1}^{n} \alpha_i(\bar{x}) \langle f(x_i), f(\cdot) \rangle_{\mathbb{R}^d} \right\rangle_{\mathcal{H}_{\mathcal{X}}} \\
&= \sum_{i=1}^{n} \alpha_i(\bar{x}) \left\langle \langle \mathbb{E}_{p(x|\bar{x})} f(x), f(\cdot) \rangle_{\mathbb{R}^d}, \langle f(x_i), f(\cdot) \rangle_{\mathbb{R}^d} \right\rangle_{\mathcal{H}_{\mathcal{X}}} \\
&\stackrel{(1)}{=} \sum_{i=1}^{n} \alpha_i(\bar{x}) \langle \mathbb{E}_{p(x|\bar{x})} f(x), f(x_i) \rangle_{\mathbb{R}^d} \\
&= \langle \mu_{\bar{x}}, \hat{\mu}_{\bar{x}} \rangle_{\mathbb{R}^d}
\end{aligned}
$$

(1) holds by the reproducing property of kernel $K_{\mathcal{X}}$ in $\mathcal{H}_{\mathcal{X}}$. We can similarly obtain:

$$
\begin{aligned}
\|m_{\bar{x}}\|_{\mathcal{H}_{\mathcal{X}}}^2 &= \left\langle \mathbb{E}_{p(x|\bar{x})} \langle f(x), f(\cdot) \rangle_{\mathbb{R}^d}, \mathbb{E}_{p(x|\bar{x})} \langle f(x), f(\cdot) \rangle_{\mathbb{R}^d} \right\rangle_{\mathcal{H}_{\mathcal{X}}} \\
&\stackrel{(1)}{=} \langle \mathbb{E}_{p(x|\bar{x})} f(x), \mathbb{E}_{p(x|\bar{x})} f(x) \rangle_{\mathbb{R}^d} \\
&= \|\mathbb{E}_{p(x|\bar{x})} f(x)\|^2 = \|\mu_{\bar{x}}\|^2
\end{aligned}
$$

Again, (1) by reproducing property of $K_{\mathcal{X}}$. And finally:

$$
\begin{aligned}
\|\hat{m}_{\bar{x}}\|_{\mathcal{H}_{\mathcal{X}}}^2 &= \left\langle \sum_{i=1}^{n} \alpha_i(\bar{x}) \langle f(x_i), f(\cdot) \rangle_{\mathbb{R}^d}, \sum_{i=1}^{n} \alpha_i(\bar{x}) \langle f(x_i), f(\cdot) \rangle_{\mathbb{R}^d} \right\rangle_{\mathcal{H}_{\mathcal{X}}} \\
&= \sum_{i,j} \alpha_i(\bar{x}) \alpha_j(\bar{x}) \langle f(x_i), f(x_j) \rangle_{\mathbb{R}^d} \\
&= \|\hat{\mu}_{\bar{x}}\|_{\mathbb{R}^d}^2
\end{aligned}
$$

By pooling these 3 equalities, we have:

$$
\begin{aligned}
\|m_{\bar{x}} - \hat{m}_{\bar{x}}\|_{\mathcal{H}_{\mathcal{X}}}^2 &= \|m_{\bar{x}}\|^2 + \|\hat{m}_{\bar{x}}\|^2 - 2\langle m_{\bar{x}}, \hat{m}_{\bar{x}} \rangle \\
&= \|\mu_{\bar{x}}\|^2 + \|\hat{\mu}_{\bar{x}}\|^2 - 2\langle \mu_{\bar{x}}, \hat{\mu}_{\bar{x}} \rangle \\
&= \|\mu_{\bar{x}} - \hat{\mu}_{\bar{x}}\|_{\mathbb{R}^d}^2
\end{aligned}
$$

We can conclude since $\|m_{\bar{x}} - \hat{m}_{\bar{x}}\| \leq O(\lambda + (n\lambda)^{-1/2})$.

E.8. Generalization bound under extended intra-class connectivity hypothesis

Theorem. Assuming 2 and 1 holds for a reproducible kernel $K_{\bar{\mathcal{X}}}$ and augmentation distribution $\mathcal{A}$. Let $f \in \mathcal{F}$ ϵ'-aligned. Let $(\bar{x}_i)_{i \in [1..n]}$ be n samples iid drawn from $p(\bar{x})$. We have:

$$\mathcal{L}_{unif}^{de}(f) \leq \mathcal{L}_{unif}^{sup}(f) \leq \mathcal{L}_{unif}^{de}(f) + 4D(2\epsilon' + \beta_n(K_{\bar{\mathcal{X}}})\epsilon) + O(n^{-1/4}) \tag{12}$$

where $\beta_n(K_{\bar{\mathcal{X}}}) = (\frac{\lambda_{min}(K_n)}{\sqrt{n}} + \sqrt{n}\lambda)^{-1} = O(1)$ for $\lambda = O(\frac{1}{\sqrt{n}})$, $K_n = (K_{\bar{\mathcal{X}}}(\bar{x}_i, \bar{x}_j))_{i,j \in [1..n]}$ and D is the maximal diameter for all $\tilde{G}_y, y \in \mathcal{Y}$. We noted $\lambda_{min}(K_n)$ is the minimal eigenvalue of K_n.

PROOF. Let $y \in \mathcal{Y}$ and $\bar{x}, \bar{x}' \sim p(\bar{x}|y)p(\bar{x}'|y)$. By Assumption 1, it exists a path of length $p \leq D$ connecting $\bar{x}, \bar{x}'$ in $\tilde{G}$. So it exists $(\bar{u}_i)_{i \in [1..p+1]} \in \bar{\mathcal{X}}$ and $(u_i)_{i \in I} \in \mathcal{X}$ s.t $\forall i \in I, u_i \sim \mathcal{A}(u_i|\bar{u}_i) \cap \mathcal{A}(u_i|\bar{u}_{i+1})$ and $\forall j \in J, \max(K(\bar{u}_j, \bar{u}_j), K(\bar{u}_{j+1}, \bar{u}_{j+1})) - K(\bar{u}_j, \bar{u}_{j+1}) \leq \epsilon$ with (I, J) a partition of $[1..p]$. Furthermore, $\bar{u}_1 = \bar{x}$ and $\bar{u}_{p+1} = \bar{x}'$. As a result, we have:

$$||\mu_{\bar{x}} - \mu_{\bar{x}'}|| = ||\mu_{\bar{u}_1} - \mu_{\bar{u}_p}||$$

$$= ||\sum_{i=1}^{p} \mu_{\bar{u}_{i+1}} - \mu_{\bar{u}_i}||$$

$$\leq \sum_{i=1}^{p} ||\mu_{\bar{u}_{i+1}} - \mu_{\bar{u}_i}||$$

$$= \sum_{i \in I} ||\mu_{\bar{u}_{i+1}} - \mu_{\bar{u}_i}|| + \sum_{j \in J} ||\mu_{\bar{u}_{j+1}} - \mu_{\bar{u}_j}||$$

Edges in E. As in proof of Theorem 1, we use the ϵ'-alignment of f to derive a bound:

$$\sum_{i \in I} ||\mu_{\bar{u}_{i+1}} - \mu_{\bar{u}_i}|| = \sum_{i \in I} ||\mu_{\bar{u}_{i+1}} - f(u_i) + f(u_i) - \mu_{\bar{u}_i}||$$

$$\leq \sum_{i \in I} ||\mu_{\bar{u}_{i+1}} - f(u_i)|| + ||f(u_i) - \mu_{\bar{u}_i}||$$

$$\overset{(1)}{\leq} \sum_{i \in I} \mathbb{E}_{p(u|\bar{u}_{i+1})}||f(u) - f(u_i)|| + \mathbb{E}_{p(u|\bar{u}_i)}||f(u_i) - f(u)||$$

$$\overset{(2)}{\leq} \sum_{i \in I}(\epsilon' + \epsilon') = 2\epsilon'|I|$$

(1) holds by Jensen's inequality and (2) because f is ϵ'-aligned.

Edges in E_K For this bound, we will use Theorem 2 to approximate $\mu_{\bar{u}}$ and then derive a bound from the property of G_K^ϵ. Let $(x_k)_{k \in [1..n]} \sim p(x_k|\bar{x}_k)$ n samples iid. By Theorem 2, we know that, for all $j \in J$, $\hat{\mu}_{\bar{u}_j}$ converges to $\mu_{\bar{u}_j}$ with ℓ_2 norm at rate $O(n^{-1/4})$ where $\hat{\mu}_{\bar{u}_j} = \sum_{k,l=1}^{n} \alpha_{k,l}K_{\bar{\mathcal{X}}}(\bar{x}_l, \bar{u}_j)f(x_k)$ and $\alpha_{k,l} = [(K_n + n\lambda\mathbf{I}_n)^{-1}]_{k,l}$. As a result, for any $j \in J$, we have:

$$||\mu_{\bar{u}_{j+1}} - \mu_{\bar{u}_j}|| = ||\mu_{\bar{u}_{j+1}} - \hat{\mu}_{\bar{u}_{j+1}} + \hat{\mu}_{\bar{u}_{j+1}} - \hat{\mu}_{\bar{u}_j} + \hat{\mu}_{\bar{u}_j} - \mu_{\bar{u}_j}||$$

$$\leq ||\mu_{\bar{u}_{j+1}} - \hat{\mu}_{\bar{u}_{j+1}}|| + ||\hat{\mu}_{\bar{u}_{j+1}} - \hat{\mu}_{\bar{u}_j}|| + ||\hat{\mu}_{\bar{u}_j} - \mu_{\bar{u}_j}|| \quad \overset{(1)}{\leq} O\left(\frac{1}{n^{1/4}}\right) + ||\hat{\mu}_{\bar{u}_{j+1}} - \hat{\mu}_{\bar{u}_j}||$$

Where (1) holds by Theorem 2. Then we will need the following lemma to conclude:

Lemma. For any $a, b, c \in \bar{\mathcal{X}}, \max(K(a,a), K(b,b)) - K(a,b) \geq |K(a,c) - K(b,c)|$ for any reproducible kernel K.

PROOF. Let $a, b, c \in \bar{\mathcal{X}}$. We consider the distance $d(x, y) = K(x, x) + K(y, y) - 2K(x, y)$ (it is a distance since K is a reproducible kernel so it can be expressed as $K(\cdot, \cdot) = \langle \phi(\cdot), \phi(\cdot) \rangle$). We will distinguish two cases.

Case 1. We assume $K(a,c) \geq K(b,c)$. We have the following triangular inequality:

$$d(a,b) + d(a,c) \geq d(b,c)$$
$$\implies K(a,b) + K(b,b) - 2K(a,b) + K(a,a) + K(c,c) - 2K(a,c) \geq K(b,b) + K(c,c) - 2K(b,c)$$
$$\implies K(a,a) - K(a,b) \geq K(a,c) - K(b,c) \geq 0$$

So $\max(K(a,a), K(b,b)) - K(a,b) \geq |K(a,c) - K(b,c)|$.

Case 2. We assume $K(b,c) \geq K(a,c)$. We apply symmetrically the triangular inequality:

$$d(a,b) + d(b,c) \geq d(a,c)$$
$$\implies K(b,b) - K(a,b) \geq K(b,c) - K(a,c) \geq 0$$

So $\max(K(a,a), K(b,b)) - K(a,b) \geq |K(a,c) - K(b,c)|$, concluding the proof.

Then, by definition of $\hat{\mu}_{\bar{u}_j}$:

$$||\hat{\mu}_{\bar{u}_{j+1}} - \hat{\mu}_{\bar{u}_j}|| = ||\sum_{k,l=1}^n \alpha_{k,l} K(\bar{x}_l, \bar{u}_{j+1}) f(x_k) - \sum_{k,l=1}^n \alpha_{k,l} K(\bar{x}_l, \bar{u}_j) f(x_k)||$$
$$= ||AC||$$

Where $A = (\sum_{k=1}^n \alpha_{kj} f(x_k)^i)_{i,j} \in \mathbb{R}^{d \times n}$ ($f(\cdot)^i$ is the i-th component of $f(\cdot)$) and $C = (K(\bar{x}_l, \bar{u}_{j+1}) - K(\bar{x}_l, \bar{u}_j))_l \in \mathbb{R}^{n \times 1}$. So, using the property of spectral ℓ_2 norm we have:

$$||\hat{\mu}_{\bar{u}_{j+1}} - \hat{\mu}_{\bar{u}_j}|| = ||AC|| \leq ||A||_2 ||C||_2$$

Using the previous lemma and because $(\bar{u}_j, \bar{u}_{j+1}) \in E_K$, we have: $||C||_2^2 = \sum_{i=1}^n (K(\bar{x}_i, \bar{u}_{j+1}) - K(\bar{x}_i, \bar{u}_j))^2 \leq \sum_{i=1}^n (\max(K(\bar{u}_{j+1}, \bar{u}_{j+1}), K(\bar{u}_j, \bar{u}_j)) - K(\bar{u}_j, \bar{u}_{j+1}))^2 \leq n\epsilon^2$. To conclude, we will prove that $||A||_2 \leq ||\alpha||_2$ where $\alpha = (\alpha_{ij})_{i,j \in [1..n]^2}$. For any $v \in \mathbb{R}^n$, we have:

$$||Av||^2 = ||\sum_{k,j=1}^n \alpha_{k,j} v_j f(x_k)||^2 \overset{(1)}{\leq} \left(\sum_{k,j=1}^n \alpha_{k,j} v_j\right)^2 = ||\alpha v||^2 \overset{(2)}{\leq} ||\alpha||_2^2 ||v||^2$$

Where (1) holds with Cauchy-Schwarz inequality and because $f(\cdot) \in \mathbb{S}^{d-1}$ and (2) holds by definition of spectral ℓ_2 norm. So we have $\forall v \in \mathbb{R}^d, ||Av|| \leq ||\alpha||_2 ||v||$, showing that $||A||_2 \leq ||\alpha||_2$.

So we can conclude that:

$$\sum_{j \in J} ||\mu_{\bar{u}_{j+1}} - \mu_{\bar{u}_j}|| \leq \sum_{j \in J} \left(\sqrt{n} ||(K_n + \lambda n \mathbf{I}_n)^{-1}||_2 \epsilon + O(n^{-1/4})\right) = |J| ||(K_n + n\lambda \mathbf{I}_n)^{-1}||_2 \sqrt{n} \epsilon + O(n^{-1/4})$$

We set $\beta_n(K_n) = \sqrt{n} ||(K_n + \lambda n \mathbf{I}_n)^{-1}||_2$. In order to see that $\beta_n(K_n) = (\frac{\lambda_{min}(K_n)}{\sqrt{n}} + \sqrt{n}\lambda)^{-1}$ with $\lambda_{min}(K_n) > 0$ the minimum eigenvalue of K_n, we apply the spectral theorem on the symmetric definite-positive kernel matrix K_n. Let $0 < \lambda_1 \leq \lambda_2 \leq ... \leq \lambda_n$ the eigenvalues of K_n. According to the spectral theorem, it exists U an unitary matrix such that $K_n = UDU^T$ with $D = \text{diag}(\lambda_1, ..., \lambda_n)$. So, by definition of spectral norm:

$$||(K_n + n\lambda \mathbf{I}_n)^{-1}||_2^2 = \lambda_{max}\left(U(D + n\lambda \mathbf{I}_n)^{-1} U^T U(D + \lambda n \mathbf{I}_n)^{-1} U^T\right)$$
$$= \lambda_{max}(U\tilde{D}U^T)$$
$$= (\lambda_1 + n\lambda)^{-2}$$

where $\tilde{D} = \text{diag}(\frac{1}{(\lambda_1 + n\lambda)^2}, ..., \frac{1}{(\lambda_n + n\lambda)^2})$. So we can conclude that $\beta_n(K_n) = (\frac{\lambda_1}{\sqrt{n}} + \sqrt{n}\lambda)^{-1} = O(1)$ for $\lambda = O(\frac{1}{\sqrt{n}})$.

Finally, by pooling inequalities for edges over E and E_K, we have:

$$||\mu_{\bar{x}} - \mu_{\bar{x}'}|| \leq 2\epsilon'|I| + |J|\beta_n(K_n)\epsilon + O(n^{-1/4}) \leq D(2\epsilon' + \beta_n(K_n)\epsilon) + O(n^{-1/4})$$

We can conclude by plugging this inequality in Theorem 7.

Theorem 4. We assume 1 and 2 hold for a reproducible kernel $K_{\bar{X}}$ and augmentation distribution $\mathcal{A}$. Let $(x_i, \bar{x}_i)_{i \in [1..n]} \sim \mathcal{A}(x_i, \bar{x}_i)$ iid samples. Let $\hat{\mu}_{\bar{x}_j} = \sum_{i=1}^n \alpha_{i,j} f(x_i)$ with $\alpha_{i,j} = ((K_n + \lambda \mathbf{I}_n)^{-1} K_n)_{ij}$ and $K_n = [K_{\bar{X}}(\bar{x}_i, \bar{x}_j)]_{i,j \in [1..n]}$. Then the empirical decoupled uniformity loss $\hat{\mathcal{L}}_{unif}^{de} \stackrel{\text{def}}{=} \log \frac{1}{n(n-1)} \sum_{i,j=1}^n \exp(-||\hat{\mu}_{\bar{x}_i} - \hat{\mu}_{\bar{x}_j}||^2)$ verifies, for any ϵ'-weak aligned encoder $f \in \mathcal{F}$:

$$\hat{\mathcal{L}}_{unif}^{de} - O\left(\frac{1}{n^{1/4}}\right) \leq \mathcal{L}_{unif}^{sup}(f) \leq \hat{\mathcal{L}}_{unif}^{de} + 4D(2\epsilon' + \beta_n(K_{\bar{X}})\epsilon) + O\left(\frac{1}{n^{1/4}}\right) \tag{13}$$

PROOF. We just need to prove that, for any $f \in \mathcal{F}$, $|\mathcal{L}_{unif}^{de}(f) - \hat{\mathcal{L}}_{unif}^{de}(f)| \leq O(n^{-1/4})$ and we can conclude through the previous theorem. We have:

$$|\mathcal{L}_{unif}^{de}(f) - \hat{\mathcal{L}}_{unif}^{de}(f)| = \left| \log \frac{1}{n(n-1)} \sum_{i,j=1}^n \exp(-||\hat{\mu}_{\bar{x}_i} - \hat{\mu}_{\bar{x}_j}||^2) - \mathbb{E}_{p(\bar{x})p(\bar{x}')} e^{-||\mu_{\bar{x}} - \mu_{\bar{x}'}||^2} \right|$$

$$\leq \left| \log \frac{1}{n(n-1)} \sum_{i,j=1}^n \exp(-||\hat{\mu}_{\bar{x}_i} - \hat{\mu}_{\bar{x}_j}||^2) - \log \frac{1}{n(n-1)} e^{-||\mu_{\bar{x}_i} - \mu_{\bar{x}_j}||^2} \right|$$

$$+ \left| \log \frac{1}{n(n-1)} e^{-||\mu_{\bar{x}_i} - \mu_{\bar{x}_j}||^2} - \mathbb{E}_{p(\bar{x})p(\bar{x}')} e^{-||\mu_{\bar{x}} - \mu_{\bar{x}'}||^2} \right|$$

The second term in last inequality is bounded by $O(\frac{1}{\sqrt{n}})$ according to property 1. As for the first term, we use the fact that $\log$ is k-Lipschitz continuous on $[e^{-4}, 1]$ and $\exp$ is k'-Lipschitz continuous on $[-4, 0]$ so:

$$\left| \log \frac{1}{n(n-1)} \sum_{i,j=1}^n e^{-||\hat{\mu}_{\bar{x}_i} - \hat{\mu}_{\bar{x}_j}||^2} - \log \frac{1}{n(n-1)} e^{-||\mu_{\bar{x}_i} - \mu_{\bar{x}_j}||^2} \right| \leq \frac{k}{n(n-1)} \left| \sum_{i,j=1}^n e^{-||\hat{\mu}_{\bar{x}_i} - \hat{\mu}_{\bar{x}_j}||^2} - e^{-||\mu_{\bar{x}_i} - \mu_{\bar{x}_j}||^2} \right|$$

$$\leq \frac{kk'}{n(n-1)} \left| \sum_{i,j=1}^n ||\hat{\mu}_{\bar{x}_i} - \hat{\mu}_{\bar{x}_j}||^2 - ||\mu_{\bar{x}_i} - \mu_{\bar{x}_j}||^2 \right|$$

Finally, we conclude using the boundness of $\hat{\mu}_{\bar{x}}$ and $\mu_{\bar{x}}$ by a constant C:

$$||\hat{\mu}_{\bar{x}_i} - \hat{\mu}_{\bar{x}_j}||^2 - ||\mu_{\bar{x}_i} - \mu_{\bar{x}_j}||^2 = (||\hat{\mu}_{\bar{x}_i} - \hat{\mu}_{\bar{x}_j}|| + ||\mu_{\bar{x}_i} - \mu_{\bar{x}_j}||)(||\hat{\mu}_{\bar{x}_i} - \hat{\mu}_{\bar{x}_j}|| - ||\mu_{\bar{x}_i} - \mu_{\bar{x}_j}||)$$

$$\leq 4C(||\hat{\mu}_{\bar{x}_i} - \hat{\mu}_{\bar{x}_j}|| - ||\mu_{\bar{x}_i} - \mu_{\bar{x}_j}||)$$

$$\leq 4C||\hat{\mu}_{\bar{x}_i} - \hat{\mu}_{\bar{x}_j} - (\mu_{\bar{x}_i} - \mu_{\bar{x}_j})||$$

$$\leq 4C(||\hat{\mu}_{\bar{x}_i} - \mu_{\bar{x}_i}|| + ||\hat{\mu}_{\bar{x}_j} - \mu_{\bar{x}_j}||)$$

$$= O\left(\frac{1}{n^{-1/4}}\right)$$